JHEP

Published for SISSA by Springer

Received: June 1, 2018
Accepted: November 22, 2018
Published: December 19, 2018

NNLOPS accurate predictions for W^+W^- production

Emanuele Re,[a,b] **Marius Wiesemann**[a] **and Giulia Zanderighi**[a,1]

[a] *Theoretical Physics Department, CERN, Geneva, Switzerland*
[b] *LAPTh, CNRS, Université Savoie Mont Blanc, 74940 Annecy, France*

E-mail: emanuele.re@lapth.cnrs.fr, marius.wiesemann@cern.ch, giulia.zanderighi@cern.ch

Abstract: We present novel predictions for the production of W^+W^- pairs in hadron collisions that are next-to-next-to-leading order accurate and consistently matched to a parton shower (NNLOPS). All diagrams that lead to the process $pp \to e^-\bar{\nu}_e\,\mu^+\nu_\mu + X$ are taken into account, thereby including spin correlations and off-shell effects. For the first time full NNLOPS accuracy is achieved for a $2 \to 4$ process. We find good agreement, at the 1σ level, with the W^+W^- rates measured by ATLAS and CMS. The importance of NNLOPS predictions is evident from differential distributions sensitive to soft-gluon effects and from the large impact (10% and more) of including next-to-next-to-leading order corrections on top of MiNLO. We define a charge asymmetry for the W bosons and the leptons in W^+W^- production at the LHC, which is sensitive to the W polarizations and hence can be used as a probe of new physics.

Keywords: NLO Computations, QCD Phenomenology

ArXiv ePrint: 1805.09857

[1] On leave from Rudolf Peierls Centre for Theoretical Physics, University of Oxford, 1 Keble Road, U.K.

Open Access, © The Authors.
Article funded by SCOAP[3].

https://doi.org/10.1007/JHEP12(2018)121

JHEP12(2018)121

Contents

1 Introduction

In the rich physics programme of LHC Run II major attention is given to measurements of Higgs-boson properties, the direct and indirect search for signals of new-physics phenomena, precision measurements and the extraction of Standard Model (SM) parameters. The production of W^+W^- pairs is among the most important LHC processes to study the gauge symmetry structure of electroweak (EW) interactions and of the mechanism of EW symmetry breaking in the SM. In particular, with the lack of clear signs of new physics, precision measurements have become of foremost importance to search for small deviations of SM predictions. They translate into indirect bounds on high-scale beyond-SM (BSM) models, whose effects manifest themselves in small deformations of SM predictions at lower energies. Most important in that respect are constraints on the allowed size of anomalous trilinear gauge couplings (aTGCs), which appear already in the leading perturbative contributions to W^+W^- production. In addition, W^+W^- final states are irreducible background to Higgs-boson measurements and to direct searches for BSM particles decaying into leptons, missing energy, and/or jets.

The W^+W^- cross section has been measured at both the Tevatron [1, 2] and the LHC (at 7 TeV [3, 4], 8 TeV [5–8] and 13 TeV [9, 10]). W^+W^- measurements, in particular with new data becoming continuously available in Run II and beyond, play a major role as SM precision tests and in constraining BSM physics, as any small deviation from the SM predictions for the production rate or the shape of distributions could be a signal of new physics. The high sensitivity to aTGCs of the W^+W^- process renders W^+W^- measurements a

JHEP12(2018)121

powerful tool for indirect BSM searches [3, 4, 6, 8, 11].[1] In the context of Higgs-boson measurements in the $H \to W^+W^-$ channel, the irreducible W^+W^- background has been extensively studied in refs. [21–28].

Measurements of continuum production of W^+W^- pairs are not the only case for which accurate predictions for this process are needed: since a complete reconstruction of the W-boson momenta is prevented by the presence of two neutrinos in the W^+W^- signature, any experimental study which features W^+W^- production as an irreducible background requires a proper modelling of the W^+W^- signal. In particular, this affects the sensitivity to $H \to W^+W^-$ and to any BSM resonance decaying into W^+W^- pairs. Apart from that, experimental analyses for both continuum W^+W^- production and Higgs-boson production in the $H \to W^+W^-$ channel organize their measurements in categories according to jet multiplicities. A rather strict veto against jet radiation is particularly important in that respect to limit the severe signal contamination due to backgrounds involving top-quarks ($t\bar{t}$ and tW). The fact that the fiducial phase-space definition involves cuts on the presence of the associated jet activity induces an increased sensitivity to higher-order QCD effects due to potentially large logarithms. Such terms challenge the reliability of fixed-order predictions in QCD perturbation theory and cause a significant increase of the uncertainty related to the extrapolation from the fiducial to the total phase space in measurements of the inclusive W^+W^- cross section. These issues show the relevance of fully flexible, hadron-level Monte Carlo predictions with state-of-the-art perturbative precision for the W^+W^- production process.

An enormous effort has been put into the computation of highly accurate predictions for W^+W^- production in the past years. Leading order (LO) [29] and next-to-LO (NLO) [30, 31] predictions for stable W bosons have been evaluated a long time ago. More sophisticated parton-level computations at NLO have become available incorporating leptonic W decays with off-shell effects and spin correlations [32–35]. Recently, also NLO electroweak (EW) corrections have been computed in both the on-shell approximation [36–38] and including the full off-shell treatment of the W bosons [39]. Although EW effects have a minor impact on the inclusive W^+W^- rate, they can be significantly enhanced up to several tens of percent at transverse momenta of about 1 TeV.

In light of sizable $\mathcal{O}(\alpha_s)$ effects, higher-order QCD corrections to W^+W^- production are indispensable to ensure highly accurate theoretical predictions for this process. W^+W^- production in association with one, two, and three jets has been computed at NLO QCD in refs. [40–43], refs. [44, 45], and ref. [46], respectively. The simplest $\mathcal{O}(\alpha_s^2)$ contribution to the W^+W^- cross section constitutes the loop-induced $gg \to W^+W^- + X$ subprocess, which receives an enhancement from the gluon luminosities and is an important part of the full next-to-NLO (NNLO) QCD corrections. $gg \to W^+W^-$ predictions at LO have been extensively studied in refs. [35, 47–50], while the Higgs-interference contribution has been considered in ref. [51]. The corresponding calculation for loop-induced $gg \to W^+W^-$+1-jet production has been presented in ref. [52].

[1] See also refs. [12–20] as examples of theory ideas to exploit precision in diboson processes to constrain BSM physics.

JHEP12(2018)121

Employing the two-loop helicity amplitudes for $gg \to VV'$ [53, 54], NLO QCD corrections to this subprocess keeping only contributions with gg initial states were computed in ref. [55] and have been extended by the inclusion of the Higgs-boson interference in ref. [56]. The complete NLO QCD corrections for $gg \to W^+W^-$ including also the gq channel are still unknown.

The full NNLO corrections to W^+W^- production have been calculated for both the inclusive cross section in the on-shell approximation [57] and the fully differential cross section incorporating leptonic W-boson decays with off-shell effects and spin correlations [58]. These computations employed the two loop helicity amplitudes of refs. [59–61]. It was found that NNLO QCD corrections have a significant impact on the inclusive cross section of roughly 10%. Contrary to what was widely expected, the dominant correction is given by the NNLO corrections to the quark-initiated process, with the size of the loop-induced gg contribution being only about 30% of the $\mathcal{O}(\alpha_s^2)$ terms. This highlights the importance of including the full NNLO corrections to this process.

Several Monte Carlo predictions have been obtained in the past years: W^+W^- production was part of the original proof-of-concept publication of the MC@NLO formalism [62] to match NLO QCD predictions with parton showers (NLO+PS); it was followed by independent NLO+PS computations in Herwig++ [63], Sherpa [64] and Powheg-Box [65, 66]. The recent Herwig7 implementation [67, 68] includes also single-resonant and gluon-induced contributions, and supersedes the previous Herwig++ prediction. More recently, also merged computations for W^+W^-+0, 1 jets at NLO+PS have become available[2] in the MEPS@NLO approach [70, 71] within OpenLoops+Sherpa [72], in the FxFx scheme [73] within MadGraph5_aMC@NLO [74], and in the MiNLO procedure [75, 76] within POWHEG BOX [77–79] through the WWJ-MiNLO generator [80]. The MiNLO computation has the advantage of being NLO accurate in both 0- and 1-jet quantities simultaneously, while other multi-jet merging simulations partition the phase space into different jet bins according to some merging scale, which spoils NLO accuracy in certain phase space regions.

State-of-the-art resummation techniques have been used to compute all higher-order logarithmic contributions up to NNLL+NLO for threshold logarithms [81] and up to NNLL+NNLO for the transverse momentum (p_T) of the W^+W^- pair [82] as well as the jet-vetoed cross section [83].[3] The latter results show that high theoretical control on the cross section with a veto on the p_T of the W^+W^- pair or on the jets can be obtained only by combining both NNLO accuracy at fixed order and resummation of large logarithmic terms. Indeed, some tension observed in earlier W^+W^- measurements [5, 7] triggered a discussion on the proper modelling of the jet-vetoed cross sections [83, 87–89] and challenged the validity of lower-order Monte Carlo predictions. Hence, a combination of parton-shower resummation with state-of-the-art perturbative precision is crucial to obtain highly accurate predictions for the production of W^+W^- pairs at the LHC.

In this paper we present a novel computation of NNLO-accurate predictions matched to parton showers (NNLOPS) for W^+W^- production at hadron colliders. More precisely, we consider all topologies which lead to two opposite-charge leptons and two neutrinos in the

[2] For a combination of fixed-order NLO predictions of W^+W^-+0, 1 jets see ref. [69].

[3] See also refs. [84–86] for earlier, less accurate results.

JHEP12(2018)121

final state ($\ell\nu_\ell\ell'\nu_{\ell'}$), thereby taking into account off-shell effects and spin correlations. This is the first time full NNLOPS accuracy is achieved for a $2 \to 4$ process. Our computation is based on the combination of two earlier computations: we start from the WWJ-MiNLO implementation [80] within the POWHEG BOX framework [77–79] and combine it with the NNLO predictions of ref. [58] which are publicly available within the Matrix code [90, 91]. To obtain NNLOPS accuracy from these two ingredients we follow the reweighting procedure used in refs. [92–95]. To handle the significantly increased complexity inherent to an off-shell diboson process with four final-state leptons we devise a parametrization of the Born-level phase space which allows us to reduce the number of degrees of freedom. In particular, we derive a formula to describe the angular dependence of the decay products of the two vector bosons in terms of spherical harmonics, which is deduced from the known expression for the decay of a single vector boson [96].

Our NNLOPS computation is implemented and will be made publicly available within the POWHEG BOX framework [77–79].[4] All-order, higher-twist, and non-perturbative QCD effects can be approximated through the interface to a parton shower using hadronization and underlying event models, which render a complete and realistic event simulation feasible. Such corrections can have a non-negligible impact on certain observables. For instance, exclusive jet cross sections can be considerably modified because of migration effects. In our implementation and throughout this paper we omit the loop-induced gg component, since it is already known to higher-order in QCD in the pure gg channel and can be added at LO+PS through known tools, such as the gg2ww event generator [50, 97] (as used by ATLAS and CMS).[5] Furthermore, in order to define W^+W^- signal events free of top-quark contamination we employ the four-flavour scheme with massive bottom quarks and drop all contributions with bottom quarks in the final state. It has been shown in refs. [57, 58] for both total and fiducial rates at NNLO that this approach is in very good agreement ($\sim$ 1–2%) with an alternative procedure to obtain top-free W^+W^- predictions in the five-flavour scheme. The latter exploits the resonance structure of top-quark contributions to fit the part of the cross section independent of the top-quark width.

Besides an extensive validation of our NNLOPS results, we study the impact of the parton shower on NNLO predictions and show the importance of including NNLO corrections on top of the MiNLO computation. In particular, the NNLOPS predictions provide new insights on the size of jet-veto logarithms at higher orders. We also compare our predictions against measurements of the total and fiducial cross sections as measured by ATLAS and CMS, and present distributions in the presence of experimental selection cuts in the fiducial volume of W^+W^- measurements. We finally use differences observed in the rapidities of the two W bosons to define a charge asymmetry for W^+W^- production and study to what extent such asymmetry remains when considering the rapidities of the two charged leptons instead.

The manuscript is organized as follows. In section 2 we describe technical aspects of the computation, including a discussion of the top-quark contamination (section 2.1), the

[4] Instructions to download the code can be obtained at http://powhegbox.mib.infn.it.

[5] A NLO+PS generator for $gg \to W^+W^-$ production could be obtained along the lines of ref. [98].

JHEP12(2018)121

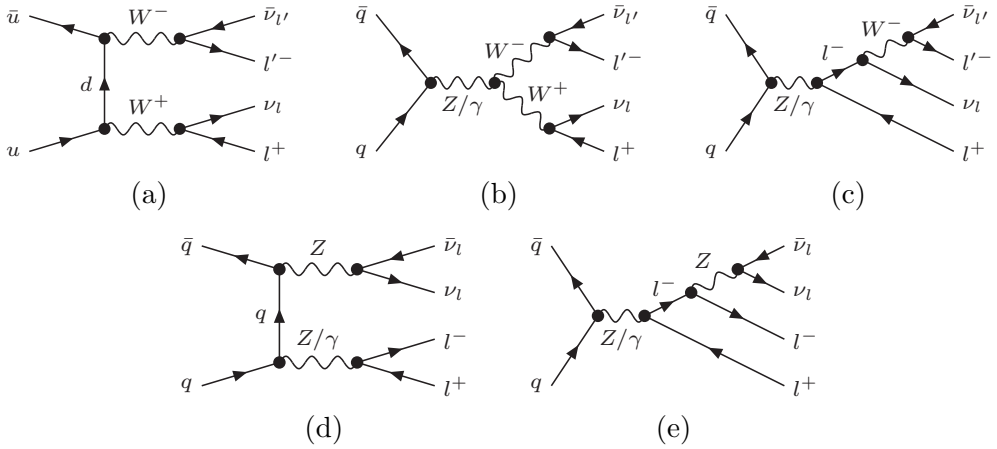

Figure 1. Born-level Feynman diagrams for W^+W^- production: (a-c) contribute to both the DF channel ($\ell \neq \ell'$) and the SF channel ($\ell = \ell'$); (d-e) only contribute in the SF case.

reweighting method to obtain NNLOPS predictions (section 2.2), its practical implementation (section 2.3), and a validation of our NNLOPS results (section 2.4). Phenomenological results are presented in section 3: we first outline input parameters and fiducial cuts (section 3.1); report cross-section predictions and compare them to data (section 3.2); study the impact of jet-veto logarithms at NNLOPS (section 3.3); demonstrate the importance of NNLOPS predictions in the fiducial phase space (section 3.4); and finally define a charge asymmetry for W^+W^- production (section 3.5). We summarize our findings in section 4.

2 Description of the calculation

We consider the production of two opposite-charge leptons and two neutrinos in proton-proton collisions

$$pp \to \ell^- \bar{\nu}_\ell \, \ell'^+ \nu_{\ell'} + X, \tag{2.1}$$

where the two leptons are of different flavour ($\ell \neq \ell'$). Our computation includes off-shell effects and spin correlations by taking into account all the resonant and non-resonant topologies leading to this process. For convenience, we simply refer to it as W^+W^- production in the upcoming sections. Already at LO these topologies involve different combinations of vector-boson resonances, such as double-resonant t-channel W^+W^- production; double-resonant s-channel W^+W^- production via Z or γ^*; and single-resonant DY-like topologies with subsequent decay. The relevant Born-level diagrams are shown in figure 1 (a-c).

While the same type of diagrams contribute also to the same-flavour (SF) case ($\ell = \ell'$), this channel involves additional topologies depicted in figure 1 (d-e): double-resonant t-channel ZZ production; and single-resonant DY-like topologies. The SF channel therefore mixes double-resonant ZZ and W^+W^- contributions. It was shown in refs. [65, 99], however, that interference effects between ZZ and W^+W^- topologies are generally small, so that the two processes can be computed separately and added incoherently. Thus, we focus on W^+W^- production in the different-flavour (DF) channel in what follows. More precisely, while our computation is applicable to any combination $\ell, \ell' \in \{e, \mu, \tau\}$ of two

JHEP12(2018)121

massless leptons of different flavour, for the sake of simplicity, we will study the process $pp \to e^- \bar{\nu}_e \, \mu^+ \nu_\mu + X$ and its charge conjugate in section 3.

2.1 Top-quark contamination in W^+W^- production

W^+W^- production is subject to a severe contamination from top-quark contributions with $t \to Wb$ decays, which enter radiative corrections through interference with real-emission diagrams featuring final-state bottom quarks. Such contributions ought to be removed to define a top-free W^+W^- cross section. Without a consistent removal of the top-quark contamination, the W^+W^- cross section, in particular in the inclusive phase space, can be increased by even an order of magnitude upon inclusion of radiative corrections, thereby corrupting the convergence of the perturbative expansion. Two approaches have been followed in the literature to compute the top-subtracted W^+W^- cross section, which will be described below. The two methods have been shown to agree within $\sim$ 1–2% for both the inclusive case [57] and with fiducial cuts [58].

In the five-flavour scheme (5FS) bottom quarks are treated as massless and appear as both initial and final-state particles. In this scheme, the presence of real bottom-quark emission is inevitably tied to $g \to b\bar{b}$ splittings in the virtual corrections through collinear singularities. Hence, such contributions must not be separated to guarantee infrared (IR) safety. Instead, the scaling behaviour of the cross sections in the limit of a vanishing top-quark width can be exploited to determine all contributions free from top-quark resonances. This approach requires the repeated computation of the cross section for varying top-quark widths in the limit $\Gamma_t \to 0$ in order to fit the resonance structure and isolate double-resonant (single-resonant) contributions, which depend quadratically (linearly) on $1/\Gamma_t$, while top-free W^+W^- contributions have no enhancement at small Γ_t. In the four-flavour scheme (4FS), on the other hand, bottom quarks are treated as massive and bottom quarks appear only as final-state particles. The bottom mass renders all partonic subprocesses with bottom quarks in the final state separately finite. The top-quark contamination in the 4FS can simply be avoided by dropping all such contributions from the computation, which are then considered part of the (off-shell) top-pair background. For convenience, we employ this approach in the calculation and throughout this paper.

2.2 NNLOPS method

Our computation of NNLO-accurate parton shower predictions for W^+W^- production builds upon two recent computations for this process: the fully differential NNLO corrections for W^+W^- production, which were calculated in ref. [58] and have become available in the Matrix framework [90, 91], and a MiNLO computation for W^+W^-+jet production in the POWHEG BOX [77–79] (WWJ-MiNLO), which was presented in ref. [80].

Matrix is a computational framework, which features NNLO QCD corrections to a large number of hadron-collider processes with color-neutral final states. This code (and earlier versions of it) has been used to obtain several state-of-the-art NNLO predictions, in particular for $Z\gamma$ [100, 101], $W^\pm\gamma$ [101], ZZ [102, 103], W^+W^- [57, 58], $W^\pm Z$ [104,

JHEP12(2018)121

105] and HH [106, 107] production.[6] MATRIX uses a fully general implementation of the q_T-subtraction formalism [108] to achieve NNLO accuracy, in combination with an automated implementation of the Catani-Seymour dipole subtraction method [109, 110] within the Monte Carlo program MUNICH[7] [113]. All (spin- and colour-correlated) tree-level and one-loop amplitudes are obtained from OPENLOOPS[8] [118–120], while dedicated computations of the two-loop amplitudes are employed [61, 121–123]. Most importantly, the two-loop amplitudes for the production of a pair of off-shell massive vector bosons [61] are taken from the publicly available code VVAMP [124], which enters our computation for W^+W^- production.

The WWJ-MINLO computation of ref. [80] implements W^+W^-+jet production within the POWHEG BOX framework and upgrades it by the MINLO procedure. As described in ref. [80], all tree-level matrix elements have been obtained using the POWHEG BOX interface to MADGRAPH v4 [125, 126], while the one-loop amplitudes have been obtained using GOSAM 2.0 [127]. The MINLO procedure merges W^+W^-+0, 1-jet multiplicities to obtain fully exclusive hadron-level events with NLO accuracy. In particular, the inclusion of a numerical implementation of the B_2 resummation coefficient, ensures that observables inclusive over the extra jet are also NLO accurate. In fact, the WWJ-MINLO computation of ref. [80] was the first to implement this approach for a genuine $2 \to 2$ process, with non-trivial virtual corrections.

To obtain NNLOPS accurate predictions from these two ingredients we follow closely the method which has already been successfully applied in the computations of Higgs [92], Drell-Yan [94], $HW^{\pm}$ [95] and HZ [128] production: the Les Houches events (LHE) produced with the WWJ-MINLO generator are reweighted to the correct NNLO prediction fully differentially in the Born phase space. This is done by means of a multidifferential reweighting covering the entire phase-space of the colourless system $(e^-\bar{\nu}_e\,\mu^+\nu_\mu)$ at LO. In its simplest form, the reweighting proceeds as follows: for each MINLO event, the reweighting factor is computed as the ratio of the NNLO cross section in the given configuration of the Born-level variables and the original MINLO weight associated with the Born-level variables of the respective event:

$$\mathcal{W}(\Phi_{\mathrm{B}}) = \frac{\mathrm{d}\sigma^{\mathrm{NNLO}}/\mathrm{d}\Phi_{\mathrm{B}}}{\mathrm{d}\sigma^{\mathrm{MiNLO}}/\mathrm{d}\Phi_{\mathrm{B}}}\,. \tag{2.2}$$

$\mathrm{d}\sigma^{\mathrm{NNLO}}/\mathrm{d}\Phi_{\mathrm{B}}$ is a multi-differential distribution obtained from the NNLO computation, while $\mathrm{d}\sigma^{\mathrm{MiNLO}}/\mathrm{d}\Phi_{\mathrm{B}}$ is the same multi-differential distribution, but determined from the WWJ-MINLO events. The observables defining the multi-differential cross section are to a large extent arbitrary as long as they form a basis of the Born-level phase space (Φ_{B}). Our specific choice for W^+W^- production will be discussed in detail in section 2.3.

[6] It was also used to compute the resummed transverse-momentum spectra for ZZ and W^+W^- pairs at NNLL+NNLO in ref. [82].

[7] The Monte Carlo program MUNICH features a general implementation of an efficient, multi-channel based phase-space integration and computes both QCD and EW [111, 112] corrections to NLO accuracy for arbitrary SM processes.

[8] OPENLOOPS relies on the fast and stable tensor reduction of COLLIER [114, 115], supported by a rescue system based on quad-precision CUTTOOLS [116] with ONELOOP [117] to deal with exceptional phase-space points.

JHEP12(2018)121

By construction, this procedure promotes the WWJ-MiNLO events to be NNLO accurate in all Born-level variables. As proven in refs. [92, 94] the reweighting does not spoil the NLO accuracy of the WWJ-MiNLO computation. Also the parton shower does not interfere with the NNLO accuracy of the W^+W^- sample, which is obvious considering the fact that the second emission is generated from the POWHEG prescription keeping NLO accuracy of the W^+W^-+jet process. Only starting from the third one, parton emissions are generated by the shower, whose impact is beyond NNLO as it affects terms from $\mathcal{O}(\alpha_s^3)$ onwards. In conclusion, the reweighting procedure under consideration allows us to obtain fully differential hadron-level events, while retaining NNLO accuracy for W^+W^- production.

One should bear in mind that eq. (2.2) reflects the reweighting factor only in its simplest form. As pointed out in ref. [92] it has the disadvantage of spreading the NNLO/NLO K-factor uniformly for observables which are non-trivial starting from the W^+W^-+1-jet phase space only, such as the transverse momentum of W-boson pair ($p_{T,WW}$). Away from the singular region, such observables are described at the same formal accuracy (effectively NLO) by the W^+W^- NNLO computation and the WWJ-MiNLO generator. Hence, no improvement can be obtained for them through the reweighting procedure. On the contrary, given that the only observables that are formally NNLO accurate are those that are non-trivial at Born level, where $p_{T,WW} = 0$, it appears to be more natural to limit the range in $p_{T,WW}$ in which the reweighting takes effect to small values of $p_{T,WW}$. Indeed, this is much closer to what is done in the matching between fixed order and analytic transverse-momentum resummation of the W^+W^- system [82, 84–86]. In fact, in analytic resummation all logarithmic terms are unambiguously matched between the two contributions upon truncation at a given order in α_s. For the analytically resummed $p_{T,WW}$ spectrum at NNLL+NNLO, see ref. [82], the NNLO contribution from the two-loop virtual corrections is, roughly speaking, distributed in $p_{T,WW}$ between zero and the respective resummation scale. As a consequence, the NLO transverse momentum distribution is recovered at large $p_{T,WW}$.

Following this idea it was suggested in ref. [92] to introduce a reweighing factor that evolves smoothly to one in regions where the NNLO computation is formally only NLO accurate and thus does not improve the NLO accuracy of the MiNLO event sample:

$$\mathcal{W}\left(\Phi_{\mathrm{B}}, p_T\right) = h\left(p_T\right) \frac{\int \mathrm{d}\sigma^{\mathrm{NNLO}}\ \delta\left(\Phi_{\mathrm{B}} - \Phi_{\mathrm{B}}\left(\Phi\right)\right) - \int \mathrm{d}\sigma_{\mathrm{B}}^{\mathrm{MiNLO}}\, \delta\left(\Phi_{\mathrm{B}} - \Phi_{\mathrm{B}}\left(\Phi\right)\right)}{\int \mathrm{d}\sigma_{\mathrm{A}}^{\mathrm{MiNLO}}\, \delta\left(\Phi_{\mathrm{B}} - \Phi_{\mathrm{B}}\left(\Phi\right)\right)} + \left(1 - h\left(p_T\right)\right) , \tag{2.3}$$

where the function $h(p_{\mathrm{T}})$ has the property that it is one at $p_T = 0$ and vanishes at infinity. This function is used in eq. (2.3) to split the cross section into

$$\mathrm{d}\sigma_{\mathrm{A}} = \mathrm{d}\sigma \cdot h(p_{\mathrm{T}}) , \qquad \mathrm{d}\sigma_{\mathrm{B}} = \mathrm{d}\sigma \cdot (1 - h(p_{\mathrm{T}})) . \tag{2.4}$$

Here we use the following smoothing function:

$$h(p_{\mathrm{T}}) = \frac{(2\,M_W)^2}{(2\,M_W)^2 + p_{\mathrm{T}}^2} . \tag{2.5}$$

JHEP12(2018)121

It is trivial to see that the exact value of the NNLO differential cross-section in the Born-level phase space is preserved using this reweighting factor:

$$\left(\frac{d\sigma}{d\Phi_{\mathrm{B}}}\right)^{\mathrm{NNLOPS}} = \left(\frac{d\sigma}{d\Phi_{\mathrm{B}}}\right)^{\mathrm{NNLO}} . \tag{2.6}$$

We have not yet specified what p_{T} exactly stands for. Between the two natural choices, the transverse momentum of the colourless system or of the leading jet, we refrain from using the former, and have chosen the transverse momentum of the leading jet instead. This choice is motivated by the fact that only the latter is a direct indicator of whether QCD radiation is present in a given event or not. This ensures that $h(p_T)$ goes to one only for Born-like configurations, while it tends to zero in the presence of hard radiation, with $\mathcal{W}(\Phi_{\mathrm{B}}, p_{\mathrm{T}})$ going to one accordingly. To define jets in $h(p_T)$ we employ the inclusive k_T-algorithm with $R = 0.4$ [129, 130] as implemented in FastJet [131].

2.3 Practical implementation

We now turn to discussing practical details on the implementation of the reweighting procedure for W^+W^- production sketched in the previous section. First we have to find a parametrization of the Born phase space. To this end, we select a set of nine independent observables, with nine being the degrees of freedom of the 4-particle ($e^-\bar{\nu}_e\ \mu^+\nu_\mu$) phase space we have at LO, after removing an overall azimuthal angle. This defines our basis for the multidimensional reweighting. We choose the variables $\Phi = \{p_{T,W^-}, y_{WW}, \Delta y_{W^+W^-}, \cos\theta^{\mathrm{CS}}_{W^+}, \phi^{\mathrm{CS}}_{W^+}, \cos\theta^{\mathrm{CS}}_{W^-}, \phi^{\mathrm{CS}}_{W^-}, m_{W^+}, m_{W^-}\}$, which correspond to the transverse momentum of W^- (that is equal and in the opposite direction to the one of W^+ at LO), the rapidity of the W^+W^- pair, the rapidity difference between the two W bosons ($\Delta y_{W^+W^-} = y_{W^+} - y_{W^-}$), the Collins-Soper (CS) angles for W^+ and W^- as introduced in ref. [96], and the invariant masses of the two W bosons, respectively. The differential cross section in the Born phase space is then defined as

$$\frac{\mathrm{d}\sigma}{\mathrm{d}\Phi_{\mathrm{B}}} = \frac{\mathrm{d}^9\sigma}{\mathrm{d}p_{T,W^-}\mathrm{d}y_{WW}\mathrm{d}\Delta y_{W^+W^-}\mathrm{d}\cos\theta^{\mathrm{CS}}_{W^+}\mathrm{d}\phi^{\mathrm{CS}}_{W^+}\mathrm{d}\cos\theta^{\mathrm{CS}}_{W^-}\mathrm{d}\phi^{\mathrm{CS}}_{W^-}\mathrm{d}m_{W^+}\mathrm{d}m_{W^-}} . \tag{2.7}$$

Given the high complexity of both the NNLO and the MiNLO computation for W^+W^- production the computation of a nine-dimensional cross section is virtually impossible with current technology. However, we can make use of two facts: first of all, we can drop the invariant W-boson masses by realizing that their differential K factor is practically flat over the whole phase space. This is true especially in the peak region of the $W^\pm$ resonances, where the majority of the events originate from, but even applies in the region where the W bosons become off-shell. Validation plots confirming this approximation are discussed in section 2.4. We therefore reduce the number of free parameters from nine to seven. Secondly, the angular dependence of each W-boson decay is fully described by the corresponding two CS angles and we exploit the fact that one can parametrize the dependence of the cross section on the CS angles for the decay of each of the W bosons in terms of the nine spherical harmonic functions $Y_{lm}(\theta^*, \phi^*)$ with $l \leq 2$ and $|m| \leq l$ [96]. This allows us to significantly simplify the calculation of the cross section in the Born

JHEP12(2018)121

phase space by expressing the sevenfold-differential distribution through the evaluation of 81 triple-differential distributions of the cross section multiplied by functions depending on the CS angles, which renders a numerical evaluation feasible.

Strictly speaking, the parametrization through CS angles is fully applicable only to double-resonant W^+W^- topologies. However, they provide by far the dominant contribution to the cross section. Indeed, the validation in section 2.4 reveals no remnants of using this procedure as an approximation in the single- and non-resonant contributions.

Before demonstrating how to express the cross section in terms of spherical harmonics of the CS angles, we briefly describe our choices of the bin sizes. For the three remaining variables[9] $\Phi_{W_*^+W_*^-} = \{p_{T,W^-},\, y_{WW},\, \Delta y_{W^+W^-}\}$, we choose bin edges:

$$\begin{aligned}
p_{T,W^-} &: \; [0., 17.5, 25., 30., 35., 40., 47.5, 57.5, 72.5, 100., 200., 350., 600., 1000., 1500., \infty]\,; \\
y_{WW} &: \; [-\infty, -3.5, -2.5, -2.0, -1.5, -1.0, -0.5, 0.0, 0.5, 1.0, 1.5, 2.0, 2.5, 3.5, \infty]\,; \\
\Delta y_{W^+W^-} &: \; [-\infty, -5.2, -4.8, -4.4, -4.0, -3.6, -3.2, -2.8, -2.4, -2.0, -1.6, -1.2, \\
&\quad -0.8, -0.4, 0.0, 0.4, 0.8, 1.2, 1.6, 2.0, 2.4, 2.8, 3.2, 3.6, 4.0, 4.4, 4.8, 5.2, \infty]\,.
\end{aligned} \tag{2.8}$$

These bins have been selected following two criteria: firstly, the bins should be sufficiently populated by events to ensure statistical robustness. Secondly, we tried to cover regions of phase space with finer binnings where the NNLO K factor features large shape effects. Not in all cases both criteria are fully compatible, in particular when there are shape effects far in the tail of distributions. The present choice constitutes a judicious compromise in these phase space regions. We will show in section 2.4 that the chosen bin edges are sufficient to obtain NNLO-accurate parton-shower predictions in all distributions and phase space regions of phenomenological interest.

We now turn to deriving a novel expression for the expansion of the cross section in spherical harmonic functions of the CS angles for a process involving the decay of two vector bosons. We start from the well-known formula for the decay of a single vector boson [96]:

$$\begin{aligned}
\frac{\mathrm{d}\sigma}{\mathrm{d}\Phi_{\mathrm{B}}} &= \frac{\mathrm{d}^7\sigma}{\mathrm{d}p_{T,W^-}\mathrm{d}y_{WW}\mathrm{d}\Delta y_{W^+W^-}\mathrm{d}\cos\theta^{\mathrm{CS}}_{W^+}\mathrm{d}\phi^{\mathrm{CS}}_{W^+}\mathrm{d}\cos\theta^{\mathrm{CS}}_{W^-}\mathrm{d}\phi^{\mathrm{CS}}_{W^-}} \\
&= \frac{3}{16\pi}\sum_{i=0}^{8} A_i\, f_i(\theta^{\mathrm{CS}}_{W^-}, \phi^{\mathrm{CS}}_{W^-}) = \frac{3}{16\pi}\sum_{i=0}^{8} B_i\, f_i(\theta^{\mathrm{CS}}_{W^+}, \phi^{\mathrm{CS}}_{W^+}),
\end{aligned} \tag{2.9}$$

where the first expansion (with A_i) corresponds to the parametrization of the W^- decay in terms of two CS angles and the second one (with B_i) is the same, but for the W^+ decay. The functions $f_i(\theta, \phi)$ are given by

$$\begin{aligned}
&f_0(\theta,\phi) = \left(1 - 3\cos^2\theta\right)/2\,, \quad f_1(\theta,\phi) = \sin 2\theta\cos\phi\,, \quad f_2(\theta,\phi) = (\sin^2\theta\cos 2\phi)/2\,, \\
&f_3(\theta,\phi) = \sin\theta\cos\phi\,, \quad f_4(\theta,\phi) = \cos\theta\,, \quad f_5(\theta,\phi) = \sin\theta\sin\phi\,, \\
&f_6(\theta,\phi) = \sin 2\theta\sin\phi\,, \quad f_7(\theta,\phi) = \sin^2\theta\sin 2\phi\,, \quad f_8(\theta,\phi) = 1 + \cos^2\theta\,.
\end{aligned} \tag{2.10}$$

[9] The star indicates that the CS angles of the respective W decays are integrated out.

JHEP12(2018)121

For $i \in \{0,\dots,7\}$ they have the property that their integral vanishes when integrating over $\mathrm{d}\cos\theta\,\mathrm{d}\phi$. The coefficients A_i and B_i are defined as moments of the differential cross section integrated over the respective CS angles:

$$\begin{aligned} A_i &= \int \frac{\mathrm{d}\sigma}{\mathrm{d}\Phi_B}\, g_i(\theta^{\mathrm{CS}}_{W^-}, \phi^{\mathrm{CS}}_{W^-})\, \mathrm{d}\cos\theta^{\mathrm{CS}}_{W^-}\mathrm{d}\phi^{\mathrm{CS}}_{W^-}\,, \\ B_i &= \int \frac{\mathrm{d}\sigma}{\mathrm{d}\Phi_B}\, g_i(\theta^{\mathrm{CS}}_{W^+}, \phi^{\mathrm{CS}}_{W^+})\, \mathrm{d}\cos\theta^{\mathrm{CS}}_{W^+}\mathrm{d}\phi^{\mathrm{CS}}_{W^+}. \end{aligned} \tag{2.11}$$

The functions $g_i(\theta,\phi)$ are defined as

$$\begin{aligned} &g_0(\theta,\phi) = 4 - 10\cos^2\theta\,, && g_1(\theta,\phi) = \sin 2\theta\cos\phi\,, && g_2(\theta,\phi) = 10\sin^2\theta\cos 2\phi\,, \\ &g_3(\theta,\phi) = 4\sin\theta\cos\phi\,, && g_4(\theta,\phi) = 4\cos\theta\,, && g_5(\theta,\phi) = 4\sin\theta\sin\phi\,, \\ &g_6(\theta,\phi) = \sin 2\theta\sin\phi\,, && g_7(\theta,\phi) = 5\sin^2\theta\sin 2\phi\,, && g_8(\theta,\phi) = 1\,. \end{aligned} \tag{2.12}$$

Note that A_8 and B_8 are actually not moments, but correspond to the differential cross section itself integrated over the respective CS angles.

With the notation that we have introduced to write eq. (2.9) in such a compact form, it is straightforward to deduce the combined formula including both decays by inserting the expression of eq. (2.9) for the W^- decay into the B_i coefficient of the W^+ decay in eq. (2.11), or vice versa. Hence, our generalization to the decay of both vector bosons for the expansion of the cross section in all four CS angles can be cast into the following form:

$$\frac{\mathrm{d}\sigma}{\mathrm{d}\Phi_{\mathrm{B}}} = \frac{9}{256\pi^2}\sum_{i=0}^{8}\sum_{j=0}^{8} AB_{ij}\, f_i(\theta^{\mathrm{CS}}_{W^-}, \phi^{\mathrm{CS}}_{W^-})\, f_j(\theta^{\mathrm{CS}}_{W^+}, \phi^{\mathrm{CS}}_{W^+})\,, \tag{2.13}$$

with coefficients

$$AB_{ij} = \int \frac{\mathrm{d}\sigma}{\mathrm{d}\Phi_B}\, g_i(\theta^{\mathrm{CS}}_{W^-}, \phi^{\mathrm{CS}}_{W^-})\, g_j(\theta^{\mathrm{CS}}_{W^+}, \phi^{\mathrm{CS}}_{W^+})\, \mathrm{d}\cos\theta^{\mathrm{CS}}_{W^-}\mathrm{d}\phi^{\mathrm{CS}}_{W^-}\mathrm{d}\cos\theta^{\mathrm{CS}}_{W^+}\mathrm{d}\phi^{\mathrm{CS}}_{W^+}\,. \tag{2.14}$$

These 81 coefficients are simply computed as triple-differential distributions of the variables $\{p_{T,W^-}, y_{WW}, \Delta y_{W^+W^-}\}$ in the Monte Carlo integration via moments of the cross section. In particular, the coefficient AB_{88} corresponds to the triple-differential cross section itself:

$$AB_{88} = \frac{\mathrm{d}^3\sigma}{\mathrm{d}p_{T,W^-}\mathrm{d}y_{WW}\mathrm{d}\Delta y_{W^+W^-}}\,. \tag{2.15}$$

In conclusion, the computation of 81 triple-differential distributions allows us to determine the fully differential cross section in the Born phase space and is feasible within both the NNLO code and the MiNLO generator.

2.4 Validation

As detailed in the previous sections, the NNLOPS procedure under consideration reweights the MiNLO events to the NNLO cross section using a set of observables spanning the Born-level phase space. Therefore, the un-showered LHE files after reweighting should match the NNLO distributions for Born-like observables up to differences caused by limited numerics.

JHEP12(2018)121

In particular, the normalization of the event sample should reproduce the inclusive NNLO cross section. In this section we provide an extensive validation of our computation for W^+W^- production by comparing LHE-level results with the nominal NNLO predictions. The NNLO results have been obtain from a statistically independent computation with respect to the one employed for the reweighting. In order to obtain all results of this paper, we have used the input parameters specified in section 3.1. For the validation plots presented here we consider the process $pp \to e^-\bar{\nu}_e\, \mu^+\nu_\mu + X$ in the inclusive phase space with no fiducial cuts.

We first point out that the inclusive NNLO cross section is reproduced to about two permille, which is at the level of the statistical uncertainties. This level of agreement can be appreciated by examining the cross-section numbers shown in table 2. We will come back to the discussion and interpretation of these numbers later.

Instead, we now turn to the discussion of differential observables. The figures of this section are organized according to the following pattern: there is a main frame, where NNLOPS (blue, solid) and MiNLO (black, dotted) results at LHE level as well as NNLO predictions (red, dashed) are shown with their absolute normalisation, and as cross section per bin (namely, the sum of the contents of the bins is equal to the total cross section, possibly within cuts). In an inset we display the bin-by-bin ratio of all the histograms which appear in the main frame over the NNLOPS curve, chosen as a reference. The vertical bars in the ratio frame indicate the statistical uncertainties on the respective prediction. The bands correspond to the residual uncertainties due to scale variations, which we compute as follows: the uncertainty of the NNLO and the MiNLO distributions are obtained by performing a variation of the renormalization ($\mu_{\rm R}$) and factorization ($\mu_{\rm F}$) scales by a factor two around the central choice subject to the restriction $1/2 \leq \mu_{\rm R}/\mu_{\rm F} \leq 2$. In the case of MiNLO the central scale choice is dictated by the MiNLO procedure: the transverse-momentum of the W^+W^- system is chosen as a scale on a point-by-point basis, and, upon integration over radiation, one recovers the inclusive cross-section with renormalization and factorization scales that scale as m_{WW}. Note that when varying the renormalization scale in the MINLO results we have also turned on the scale variation in the MINLO Sudakov form factor, see appendix B of ref. [76]. In the case of the NNLO the central scale is chosen to be the average of the transverse masses of the two W bosons, see eq. (3.1). In order to assess the uncertainty of our NNLOPS predictions, computed using eq. (2.3), we have evaluated the NNLO and MiNLO differential cross-sections using the same scale-variation factors. As a result, the uncertainty of the NNLOPS is also the envelope of a 7-point scale variation.

We begin by showing in figure 2 the three observables applied in our NNLOPS reweighting with the binning as in eq. (2.8). We see that the NNLO distributions are nicely reproduced by the NNLOPS computation. Differences are below one percent in the bulk region of the distributions and increase to the few-percent level in regions with limited numerics only. This validates the three-dimensional reweighting we used to obtain our NNLOPS results.

We next consider the CS angles of the W^+ decay. The corresponding results for the W^- decay are practically identical which is why we refrain from discussing them separately. Figure 3 shows that the distributions in $\theta^{\rm CS}_{W^+}$ and $\phi^{\rm CS}_{W^+}$ are in perfect agreement between

JHEP12(2018)121

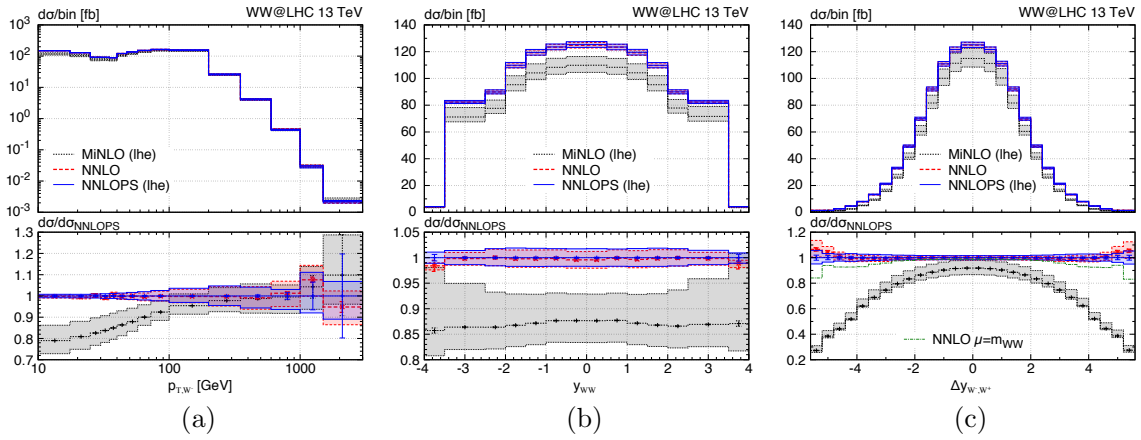

Figure 2. Comparison at LHE level of our NNLOPS results (solid, blue) with the nominal NNLO predictions (red, dashed) for the three distributions used in the reweighting, with the binning of eq. (2.8): (a) p_{T,W^-}, (b) y_{WW} and (c) $\Delta y_{W^+W^-}$; MiNLO results at the LHE level (black, dotted) are shown for reference; see text for details.

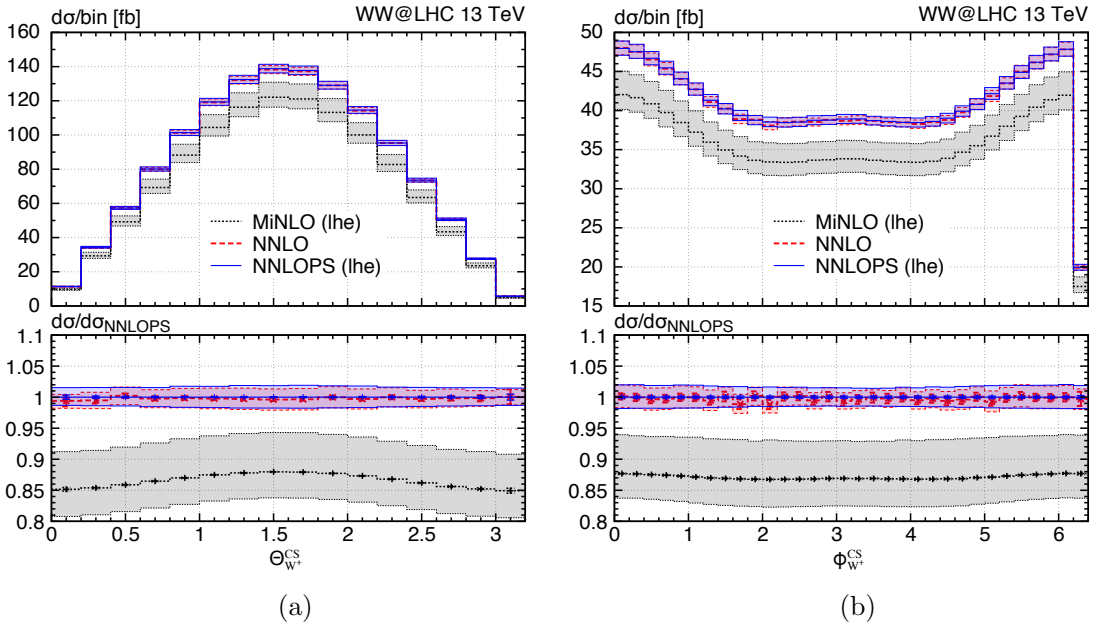

Figure 3. Same as figure 2, but for the CS angles of the W^+ decay: (a) $\theta^{CS}_{W^+}$ and (b) $\phi^{CS}_{W^+}$.

NNLOPS and NNLO, which demonstrates the validity of our procedure to describe the W decays via CS angles. In fact, we have checked explicitly at NNLO level that eq. (2.13) reproduces the correct cross section when being differential in any two of the four CS angles at the same time.

Let us add at this point that we have also tried to only use the three-dimensional reweighting in $\mathrm{d}\Phi_{W^+_*W^-_*}$ without using the CS angles by replacing

$$\frac{\mathrm{d}\sigma}{\mathrm{d}\Phi_{\mathrm{B}}} \equiv \frac{\mathrm{d}\sigma}{\mathrm{d}\Phi_{W^+_*W^-_*}} = \frac{\mathrm{d}^3\sigma}{\mathrm{d}p_{T,W^-}\mathrm{d}y_{WW}\mathrm{d}\Delta y_{W^+W^-}} \tag{2.16}$$

in eq. (2.2). As expected, this reduces some statistical fluctuations. In fact, we found

JHEP12(2018)121

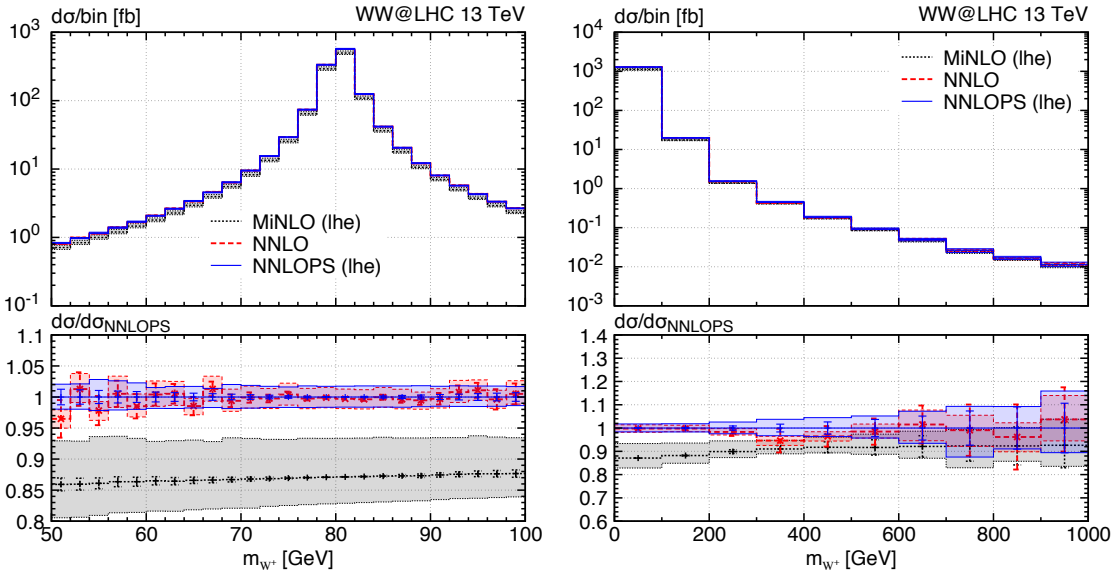

Figure 4. Same as figure 2, but for the invariant mass of the W^+ boson m_{W^+} in two different regions: (a) around the W-mass peak, $m_{W^+} \in [50, 100]$ GeV, and (b) including off-shell regions, $m_{W^+} \in [0, 1000]$ GeV.

that excluding the CS angles the NNLO distributions are still very well reproduced by the NNLOPS sample. Of all one-dimensional distributions we considered, only $\theta^{\text{CS}}_{W^+}$ and $\theta^{\text{CS}}_{W^-}$ show a mildly different shape (at the few-percent level) in this case. We therefore provide the reweighting without CS angles as an option in our code, while keeping the application of the full expression in eq. (2.13) the default in the code and throughout this paper. One must bear in mind that as soon as double differential distributions in angular observables of the leptons are considered the validity of the application of the reweighting without CS angles may be limited.

The only observables in our definition of the Born phase space, see eq. (2.7), which remain to be validated are the invariant masses of the two W bosons. We first recall that for reasons of complexity we excluded them from the Born-level variables in the reweighting procedure by assuming them to feature flat higher-order corrections. Indeed, figure 4 (a) confirms this to be an appropriate assumption in the peak-region of the spectrum, where the bulk of events is situated and the agreement of the NNLO with the NNLOPS distributions is close to perfect. Even in the phase-space areas where the two W bosons become far off-shell the NNLOPS result deviates by less than 5% from the NNLO curve, see figure 4 (b). This discrepancy is at the level of the statistical uncertainty in these regions. We note that we only show the m_{W^+} distribution in that figure, because the m_{W^-} results are practically identical.

We conclude this section by studying distributions which have not been used in the parametrization of our phase-space definition in eq. (2.7). This is important in order to convince oneself that, beyond the observables used for the reweighting, our procedure

JHEP12(2018)121

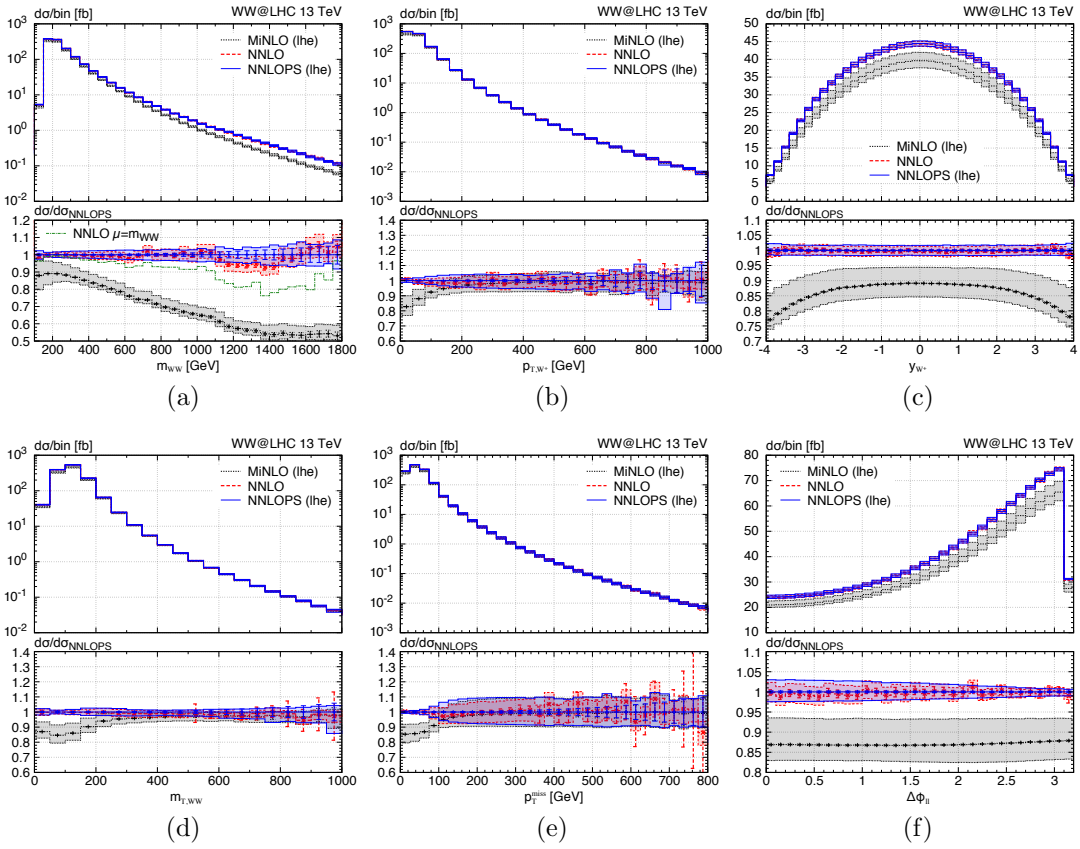

Figure 5. Same as figure 2, but for observables which have not been used in eq. (2.7) to define a basis of the Born-level phase space: (a) invariant mass of the W^+W^- pair m_{WW}, (b) transverse momentum p_{T,W^+} and (c) rapidity y_{W^+} of W^+, (d) transverse mass of the W^+W^- pair $m_{T,WW}$ defined eq. (2.17), (e) missing transverse momentum $p_T^{\rm miss}$ and (f) lepton separation $\Delta\phi_{\ell\ell}$.

reproduces correctly the NNLO cross section for other distributions. Figure 5 shows corresponding plots for the invariant mass of the W^+W^- pair, the transverse momentum and the rapidity of W^+, the transverse mass of the W^+W^- pair defined as

$$m_{T,WW} = \sqrt{\left(E_{T,\ell_1} + E_{T,\ell_2} + p_T^{\rm miss}\right)^2 - \left(\mathbf{p}_{T,l_1} + \mathbf{p}_{T,l_2} + \mathbf{p}_{\mathbf{T}}^{\rm miss}\right)^2}\,, \tag{2.17}$$

the missing transverse momentum, as well as the separation in the azimuthal angle $\Delta\phi_{ll}$ of the two charged leptons. We stress that we have considered a large number of relevant observables and that we have picked a representative set of distributions here. In particular, m_{WW} is the one we found most sensitive to statistical effects.[10] Looking at figure 5 it is clear that our reweighting procedure allows us to promote the MiNLO sample to have NNLO accuracy for Born-level observables: even in regions where the MiNLO and NNLO curves are far apart the NNLOPS predictions are perfectly consistent with the NNLO ones. This is particularly evident in the region of large m_{WW}, where the MiNLO result is

[10] One should bear in mind that the statistical error bars of the NNLOPS results originate only from the finite number of generated events. They do not contain any uncertainty related to statistical limitations in the reweighting procedure itself and to the finite bin sizes used therein.

JHEP12(2018)121

almost a factor 2 below the NNLO one. Not only the central predictions are in reasonable agreement, also the NNLOPS uncertainty bands are of the expected size, being close to the NNLO ones. The fact that upon reweighting NNLOPS agrees with the NNLO for Born-level observables verifies that the parametrization through CS angles, which, strictly speaking, is applicable only to the double-resonant W^+W^- contributions, is an excellent approximation in general.

One might wonder what is the reason for the large difference between MiNLO and NNLO at large m_{WW}. It can be easily traced back to the different scale choice in the NNLO calculation and in MiNLO. In fact, MiNLO uses effectively m_{WW} as a primary scale, which becomes a very hard scale in the tail of the m_{WW} distribution. On the contrary, the dynamic scale choice in the NNLO calculation, see eq. (3.1), is not sensitive to the rapidity distance between the two W-bosons. Hence, it can be much smaller than m_{WW} when there is a large rapidity separation between the W bosons. As expected, similar effects can be observed also in the rapidity distribution of the W^+ boson and the rapidity difference between the two W bosons, see figure 5 (c) and figure 2 (c), respectively. We note that the difference between NNLO and MiNLO would be about 20% smaller in the tail of the $\Delta y_{W^+W^-}$ and m_{WW} distributions if $\mu = m_{WW}$ was used. It is not clear which scale choice is more appropriate for W^+W^- production. For instance, if the W bosons originate from the s-channel decay of an off-shell Z boson, the invariant mass (possibly transverse mass) of the W-boson pair is the natural choice. However, through the t-channel diagrams it is also possible to emit one W boson as initial-state (soft, large rapidity) radiation and a second W boson as a standard hard Drell Yan interaction. In this case, the choice done in the NNLO calculation would be more appropriate. Since of course all topologies interfere, it seems hard to argue in favour of any of the two scale choices.

3 Results

In this section we present NNLOPS-accurate predictions for the processes $pp \to e^{\mp}\nu_e\,\mu^{\pm}\nu_\mu + X$. Hence, we consider the production of two different-flavour leptons together with the two corresponding neutrinos and its charge-conjugated process. After defining our general setup, we discuss rates and distributions both in the inclusive phase space and in presence of fiducial cuts.

3.1 Input parameters and fiducial cuts

We study predictions at the 13 TeV LHC. The G_μ scheme is employed for EW parameters and the complex-mass scheme [132] for EW decays of the W bosons. Thus, complex W- and Z-boson masses are used and the EW mixing angles are defined as $\cos\theta_W^2 = (m_W^2 - i\Gamma_W\, m_W)/(m_Z^2 - i\Gamma_Z\, m_Z)$ and $\alpha = \sqrt{2}\, G_\mu m_W^2 \sin^2\theta_W/\pi$. The input parameters are set to the PDG [133] values: $G_F = 1.16639 \times 10^{-5}\,\text{GeV}^{-2}$, $m_W = 80.385\,\text{GeV}$, $\Gamma_W = 2.0854\,\text{GeV}$, $m_Z = 91.1876\,\text{GeV}$, $\Gamma_Z = 2.4952\,\text{GeV}$, and $m_H = 125.0\,\text{GeV}$. We obtain a branching fraction of $\text{BR}(W^\pm \to \ell^\pm\nu_\ell) = 0.108987$ from these inputs for the W-boson decay into massless leptons. The CKM matrix is set to unity, which, because of unitarity and because we consider only massless external quarks, is almost equivalent to using the full

JHEP12(2018)121

Cabibbo matrix.[11] As outlined in section 2.1, we use the 4FS with massive bottom quarks throughout and consistently remove top-quark contamination by dropping all partonic subprocesses with real bottom-quark emissions, which are separately IR finite. The on-shell top- and bottom-quark masses are set to $m_t = 173.2\,\text{GeV}$ and $m_b = 4.92\,\text{GeV}$.[12] We use the NNPDF3.0 [134] $n_f = 4$ PDF sets with the corresponding value of the strong coupling constant.[13] As usual, for the fixed-order results, we choose N^{n}LO PDF sets in accordance with the perturbative order under consideration, while the evolution of α_s is done at $(n+1)$-loop order. In the WWJ-MiNLO simulation NNLO PDFs are used. We use dynamical renormalization (μ_R) and factorization (μ_F) scales: for the NNLO computation the average of the transverse masses of the two W bosons is chosen as a central scale:

$$\mu_R = \mu_F = \mu_0 \equiv \frac{1}{2}\left(\sqrt{m^2_{e^-\bar{\nu}_e} + p^2_{T,e^-\bar{\nu}_e}} + \sqrt{m^2_{\mu^+\nu_\mu} + p^2_{T,\mu^+\nu_\mu}}\right), \tag{3.1}$$

while, upon integration over all radiation, the scales in the MiNLO generator effectively reduce to an m_{WW}-like scale. As described in section 2.4, uncertainties from missing higher-order contributions are estimated from the customary 7-point variation, while keeping the μ_R and μ_F values correlated in the NNLOPS reweighting factor. All showered results are obtained through matching to the Pythia8 parton shower [135]. Results are shown at parton level, without hadronization or underlying-event effects.

Additional uncertainties connected to the shower-matching could be probed by varying the choice of $h(p_t)$ in eq. (2.3), by using different parton showers or parton-shower tunes, or by varying the shower vetoing scale by a factor of two for events with radiation far from singular limits. All these effects can be considered as uncorrelated. Their complete assessment is left for future studies. Therefore, the size of uncertainties quoted in this paper may be underestimated. However, comprehensive studies related to the shower and matching systematics can be performed with the public code.

In table 1 we summarize the set of cuts used in the definition of the fiducial phase space. They involve standard cuts on the transverse momentum ($p_{T,\ell}$) and pseudo-rapidity (η_ℓ) of the charged leptons as well as a lower threshold on the invariant-mass of the dilepton pair ($m_{\ell^-\ell^+}$). Lepton dressing with QED final-state radiation (FSR) is not included in the fiducial results shown in this paper. However, we discuss the general effects of its simulation with Pythia8 below. A typical minimal requirement on the missing transverse momentum (p_T^{miss}) is supplemented by a cut on the so-called relative missing transverse momentum ($p_T^{\text{miss,rel}}$), which denotes the component of the p_T^{miss} vector perpendicular to the direction

[11] An approximation is made in the real correction when the two W bosons are emitted from two different fermion lines, one in the initial state and one in the final state. First of all, these contributions are very small, as they contain a gluon propagator in the s-channel which is pushed far off-shell by the W boson emitted off the final state fermion line. Additionally, these effects are further suppressed by the heavy-flavour PDFs. Hence, replacing the CKM matrix by the unit matrix is a very good approximation.

[12] We note that the contributions involving massive fermion loops, which include also the exchange of a Higgs boson and appear starting from $\mathcal{O}(\alpha_s^2)$, are accounted for through the reweighting to the NNLO.

[13] The strong coupling constant of the $n_f = 4$ NNPDF set is derived from the standard variable-flavour-number PDF set with $\alpha_s^{(5\text{F})}(M_Z) = 0.118$ using an appropriate backward and forward evolution with five and four active flavours, respectively. This results in values of 0.1136, 0.1123 and 0.1123 for $\alpha_s^{(4\text{F})}(M_Z)$ at LO, NLO and NNLO.

JHEP12(2018)121

lepton cuts	$p_{T,\ell} > 25\,\text{GeV}, \quad \lvert\eta_\ell\rvert < 2.4, \quad m_{\ell^-\ell^+} > 10\,\text{GeV}$
lepton dressing	add photon FSR to lepton momenta with $\Delta R_{\ell\gamma} < 0.1$ *(our results do not include photon FSR, see text)*
neutrino cuts	$p_T^{\text{miss}} > 20\,\text{GeV}, \quad p_T^{\text{miss,rel}} > 15\,\text{GeV}$
jet cuts	anti-k_T jets with $R = 0.4$;
	$N_{\text{jet}} = 0$ for $p_{T,j} > 25\,\text{GeV}$, $\lvert\eta_j\rvert < 2.4$ and $\Delta R_{ej} < 0.3$
	$N_{\text{jet}} = 0$ for $p_{T,j} > 30\,\text{GeV}$, $\lvert\eta_j\rvert < 4.5$ and $\Delta R_{ej} < 0.3$

Table 1. Fiducial cuts used in the W^+W^- analysis by ATLAS at 13 TeV [9]. See text for details.

of the closest lepton in the azimuthal plane:

$$p_T^{\text{miss,rel}} = \begin{cases} p_T^{\text{miss}} \cdot \sin|\Delta\phi| & \text{for } \Delta\phi < \pi/2\,, \\ p_T^{\text{miss}} & \text{for } \Delta\phi > \pi/2\,, \end{cases} \tag{3.2}$$

where $\Delta\phi$ denotes the azimuthal angle between the p_T^{miss} vector and the nearest lepton. Finally, there is a two-folded jet-veto requirement: jets are rejected for a softer $p_{T,j}$ threshold in a narrow pseudo-rapidity (η_j) range, while slightly harder jets are vetoed also in a wider pseudo-rapidity range. This setup follows precisely the definition of the fiducial volume employed in the ATLAS 13 TeV W^+W^- measurement of ref. [9], which we will compare to below. We refer to this default set of fiducial cuts, which include the jet-veto requirements, as `fiducial-JV`. In the following, it will be instructive to also consider the same fiducial setup, but without any restriction on the jet activity, which we denote as `fiducial-noJV` in the respective figures.

We refrain from showing results including charged leptons dressed with photon FSR in the following, in order to allow for a more direct comparison between NNLO and the showered results. Besides, a proper treatment is closely tied to the specific choices made by the experimental collaborations. Nevertheless, for completeness we have simulated such effects by generating photon emissions with Pythia8, and successively considering dressed leptons, i.e. we added to their momentum all photon momenta in a cone of $\Delta R_{\ell\gamma} < 0.1$. By and large, the impact of photon FSR is at the level of a few percent. In particular, the cross section in the fiducial phase space is reduced by about 2%. Relatively large effects ($> 10\%$) are found only in distributions where it is expected, such as the invariant mass of each of the two W bosons or the charged lepton transverse momenta. We stress that with our NNLOPS computation the experimentalists have now a tool to produce NNLO accurate predictions, and, at the same time, to consistently include lepton dressing through photon FSR as obtained by a parton shower.

All fiducial results in this section have been obtained for the $pp \to e^-\bar{\nu}_e\,\mu^+\nu_\mu$ process, while multiplying them with a factor of two to account for the charge-conjugated process ($pp \to e^+\nu_e\,\mu^-\bar{\nu}_\mu$).[14] As pointed out in the introduction, contributions which stem from

[14] We have explicitly checked that the minor asymmetry in the electron and muon cuts, which appears only in the electron-jet separation of the jet-veto definition, has a completely negligible impact. Our procedure can therefore be considered to provide the exact result for the sum of the two (charge-conjugated) processes.

JHEP12(2018)121

$q\bar{q}$ (no loop^2 gg)	$\sigma_{\text{incl}}(pp \to W^+W^-)$ [pb]	$\sigma_{\text{fid}}(pp \to e^\mp\nu_e\,\mu^\pm\nu_\mu)$ [fb]	A $= \sigma_{\text{fid}}/\sigma_{\text{incl}}$ [%]
LO	$70.66(1)^{+5.1\%}_{-6.2\%}$	$440.5(0)^{+6.0\%}_{-7.1\%}$	0.623
NLO	$99.96(3)^{+3.5\%}_{-2.8\%}$	$411.8(1)^{+2.7\%}_{-2.3\%}$	0.412
NNLO	$110.0(1)^{+1.6\%}_{-1.6\%}$	$413.1(2)^{+1.0\%}_{-0.7\%}$	0.376
MiNLO	$96.05(1)^{+7.1\%}_{-4.9\%}$	$359.6(1)^{+5.4\%}_{-8.3\%}$	0.374
NNLOPS	$110.2(2)^{+1.7\%}_{-1.6\%}$	$413.0(2)^{+2.2\%}_{-2.3\%}$	0.375
ATLAS$-gg$ [9]	$124.7 \pm 5\,(\text{stat}) \pm 13\,(\text{syst}) \pm 3\,(\text{lumi})$	$473 \pm 20\,(\text{stat}) \pm 50\,(\text{syst}) \pm 11\,(\text{lumi})$	0.379
CMS$-gg$ [10]	$108.5 \pm 5.8\,(\text{stat})\ ^{\pm 5.7(\text{exp. syst})}_{\pm 6.4(\text{theo. syst})} \pm 3.6\,(\text{lumi})$	—	—

Table 2. Cross sections for inclusive W^+W^- production and $e^\mp\nu_e\,\mu^\pm\nu_\mu$ production with fiducial cuts in various approximations compared to data. At NNLO, all corrections to $q\bar{q}$-bar induced W^+W^- production are taken into account up to $\mathcal{O}(\alpha_s^2)$, while excluding the loop-induced gg contribution. The central values of the experimental results have been corrected by subtracting the $\mathcal{O}(\alpha_s^3)$ theoretical prediction for the (non-resonant) gg component [55] as quoted in the ATLAS analysis [9]. In contrast to CMS, ATLAS includes resonant Higgs bosons decaying to W^+W^- pairs in their W^+W^- signal measurement. The theoretical predictions of this additional gg-initiated contribution in the inclusive [136] and fiducial [136, 137] phase space as quoted in the ATLAS analysis [9] have also been removed from the central ATLAS result.[15]

the loop-induced gg channel and enter the NNLO corrections to W^+W^- production are disregarded throughout this work. We employ this simplification to perform a clean study of the newly computed NNLOPS effects. For a fully consistent comparison to data all contributions should be combined with correlated scale variations.

3.2 Inclusive and fiducial rates

In table 2, we report results for integrated cross sections, both fully inclusive and with fiducial cuts. The inclusive W^+W^- results have been obtained from the full off-shell computation of the leptonic process in eq. (2.1) by simply dividing out the branching fraction of the $W \to \ell\nu$ decays. The numbers inside the brackets after the central prediction are the numerical errors, while the percentages reflect the uncertainties due to scale variations. For reference, we also quote the acceptance obtained from the ratio of the central prediction for the fiducial cross section over the inclusive one. The predicted rates are provided in various approximations, with NNLOPS being our best prediction. All the available experimental results at 13 TeV by ATLAS and CMS are quoted in the same table. Since we omit loop-induced gg contributions in the $\mathcal{O}(\alpha_s^2)$ calculations, the central values of the measured cross sections have been corrected by removing the respective theory prediction of the gg

[15] We note that the prediction used for the inclusive Higgs results includes the N3LO cross section in the heavy-top limit of refs. [138–140] and quark-mass effects [93, 137, 141–148]. The fiducial acceptance for the resonant Higgs contributions in ref. [9] has been computed with the POWHEG implementation [137], but equivalent tools using the MC@NLO approach [149], or even more sophisticated merging [150, 151] and NNLOPS [92, 93, 152] predictions could have been used to determine the acceptance. Given the minor impact ($\sim 2\%$) of resonant Higgs contributions in the fiducial phase space, which is due to the applied jet veto, a more precise modelling of the Higgs contributions is not required.

JHEP12(2018)121

component to facilitate a meaningful comparison, as detailed in the caption of the table. The main conclusions that can be drawn from the table are the following:

1. Radiative corrections on the inclusive cross section are large. They amount to +41.4% at NLO and are still +10.0% at NNLO. The MiNLO result is, in accordance with its formal accuracy, very close to the inclusive NLO rate. By construction, NNLOPS yields the inclusive NNLO cross section up to statistics.

2. In the fiducial phase space the situation is quite different. Radiative corrections are much smaller and even negative at NLO. They amount to −6.5% at NLO and +0.32% at NNLO. In fact, looking only at the $\mathcal{O}(\alpha_s^2)$ coefficient, i.e. comparing against NLO computed with NNLO PDFs (referred to as NLO′) which yields $\sigma_{\text{fid}}^{\text{NLO}'} = 424.6(1)^{+2.5\%}_{-2.1\%}$, one realizes that the $\mathcal{O}(\alpha_s^2)$ contributions from the NNLO matrix elements are actually also negative. We stress that these findings are caused entirely by the restrictions of jet activity in the fiducial phase space. If we remove the jet-veto requirements, i.e. consider the `fiducial-noJV` setup, radiative corrections are similar to the inclusive case.

3. When comparing MiNLO and NLO results, it appears quite surprising that the two fiducial cross sections turn out to be so different, despite the fact that they are practically identical in the `fiducial-noJV` setup. However, it was pointed out some time ago [89] that the POWHEG generator tends to underestimate the jet-vetoed cross section for W^+W^- production, which seems to persist also in its MiNLO extension. When MiNLO is reweighted to the NNLO this deficit in the fiducial cross section disappears. The reasons for why this happens are twofold: first, the fiducial cross section without a jet-veto is about 10% higher at NNLO than for MiNLO; second, the jet-veto efficiency predicted by MiNLO is $\sim 5\%$ lower than at NNLOPS for relevant jet-veto cuts (see section 3.3). It shall be noted, however, that the reasonable size of the fiducial cross section at NLO is accidental. It is caused by the interplay of the small cross section without a jet veto and a poor modelling of the jet-veto efficiency. This is apparent considering the acceptance in the last column, which is rather similar among NNLO, MiNLO and NNLOPS, but quite higher at NLO.

4. It is interesting to note that the fiducial NNLOPS result is identical with the NNLO cross section, despite the fact that its description of jet-veto logarithms is more accurate at low jet-veto scales. We postpone a detailed discussion to section 3.3, where we analyze the cross section as a function of the jet-veto cut. We note, however, that the perturbative uncertainties of the NNLOPS result are more realistic than at NNLO. As expected they are larger in the restricted phase space than in the fully inclusive one, while the opposite is the case at NNLO.

5. Despite the rather small QCD corrections in the fiducial phase space, only beyond NLO a reliable prediction for the fiducial acceptance is obtained.

JHEP12(2018)121

6. As expected, scale uncertainties successively decrease upon inclusion of QCD perturbative corrections. At LO and NLO, they underestimate, however, the actual size of missing higher-order terms in the case of the inclusive cross section.

7. The agreement between the NNLO(PS) predictions and the measured cross sections is quite good. This is particularly true for the inclusive cross section, which is fully consistent with the CMS measurement within the statistical uncertainty, and agrees also with the ATLAS one as soon as systematics are taken into account. Clearly, the tension found in some early 8 TeV W^+W^- measurements of the inclusive cross section [5, 7] does not persist at 13 TeV with state-of-the-art theoretical predictions. For the fiducial cross-section measurement by ATLAS the relative difference to the NNLOPS result is somewhat higher, but still within the quoted uncertainties.

3.3 Jet-vetoed cross section and impact of the parton shower

We now consider the integrated cross section with a jet-veto as a function of the jet-veto cut (p_{T,j_1}^{veto}) defined as

$$\sigma(p_{T,j_1} < p_{T,j_1}^{\text{veto}}) = \int_0^{p_{T,j_1}^{\text{veto}}} \mathrm{d}p_{T,j_1} \frac{\mathrm{d}\sigma}{\mathrm{d}p_{T,j_1}} = \sigma_{\text{int}} - \int_{p_{T,j_1}^{\text{veto}}}^{\infty} \mathrm{d}p_{T,j_1} \frac{\mathrm{d}\sigma}{\mathrm{d}p_{T,j_1}} \,. \tag{3.3}$$

σ_{int} denotes the cross section integrated over all p_{T,j_1}. In addition to the jet-veto requirement any IR-safe set of cuts may be imposed on the cross section in the previous equation. We further define the jet-veto efficiency as

$$\varepsilon(p_{T,j_1}^{\text{veto}}) = \sigma(p_{T,j_1} < p_{T,j_1}^{\text{veto}})/\sigma_{\text{int}}. \tag{3.4}$$

Figure 6 depicts both the jet-vetoed cross section and the jet-veto efficiency in the fiducial phase space. We point out that the relative behaviour of the curves is practically identical in the fully inclusive phase space, which is why we refrain from discussing them separately, and that the general conclusions drawn here also apply in the inclusive case. The figures throughout this section follow the same pattern as in section 2.4, only that they now show in the main frame physical results for MiNLO and NNLOPS after shower, and not the ones at LHE level.

Since NNLO (red, dashed) and NNLOPS (blue, solid) have almost identical cross sections, there is virtually no difference in relative terms between their jet-vetoed cross sections and the respective efficiency. MiNLO (black, dotted), on the other hand, has a different normalization in the `fiducial-noJV` phase space of roughly -13%. Furthermore, the jet-veto efficiency predicted by MiNLO is about 4% below the NNLOPS one for typical jet-veto cuts applied by the experiments ($20\,\text{GeV} \lesssim p_{T,j_1}^{\text{veto}} \lesssim 30\,\text{GeV}$).

The agreement between NNLO and NNLOPS results is remarkable. Even down to $p_{T,j_1}^{\text{veto}} = 15\,\text{GeV}$ their difference is within $\sim 2\%$. Similar results were found in ref. [83] with resummation effects at high logarithmic accuracy of about ~ 2–3% beyond NNLO for $p_{T,j_1}^{\text{veto}} = 30\,\text{GeV}$. This shows that jet-veto logarithms at typical jet-veto cuts applied by the experiments are not particularly large and still well described by a NNLO computation.

JHEP12(2018)121

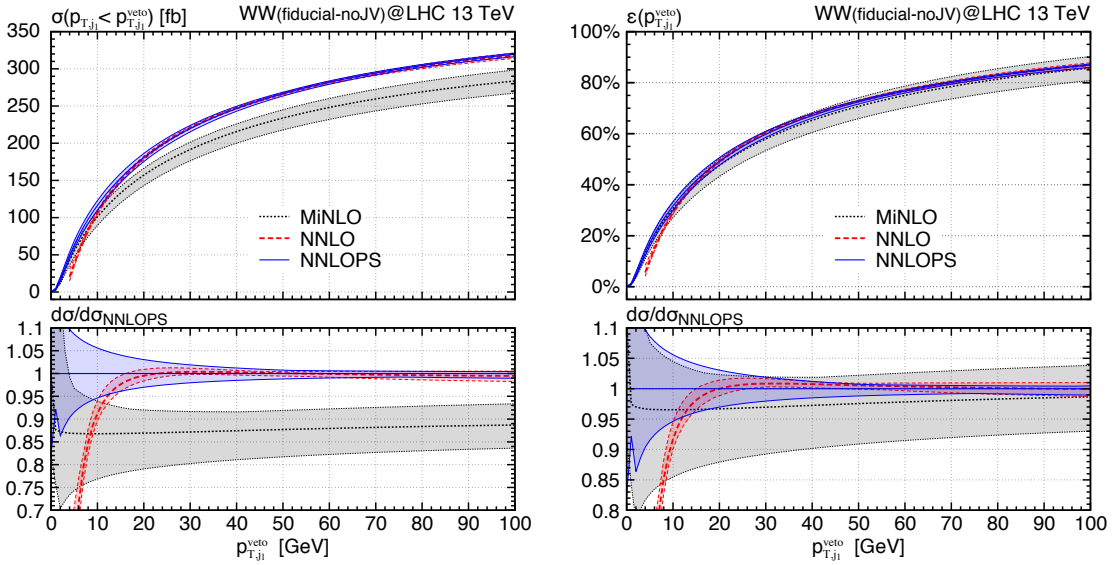

(a) (b)

Figure 6. Comparison of MiNLO (black, dotted), NNLO (red, dashed) and NNLOPS (blue, solid) predictions in the fiducial phase space as a function of p_{T,j_1}^{veto} for (a) the cross section and (b) the jet-veto efficiency.

Clearly, below $p_{T,j_1}^{\text{veto}} = 15\,\text{GeV}$ NNLO loses all predictive power and even turns negative at some point. The scale-uncertainty band completely underestimates the true uncertainty of the NNLO prediction due to missing higher-order corrections in this region. It is nice to see how matching to the parton shower cures the unphysical behaviour of the NNLO result, so that NNLOPS yields accurate predictions in the entire range of jet-veto cuts. Furthermore, the scale uncertainty band of the NNLOPS curve widens at small p_{T,j_1}^{veto}, reflecting the fact that higher-order logarithmic terms become important in this region and degrade the accuracy of the perturbative prediction.

3.4 Differential distributions in the fiducial phase space

We now turn to discussing differential cross sections. The figures in this section have the same layout as before. Additionally, we show the central NNLOPS result at LHE level, i.e. before the shower is applied, in the ratio frame. We start by considering observables which are sensitive to soft-gluon emissions. In phase-space regions where the cross section becomes sensitive to soft-gluon effects, large logarithmic terms spoil the validity of fixed-order computations and must be resummed to all orders to yield a physical description. This can be done either via analytic resummation techniques or via a parton-shower approach. Therefore, the largest and most relevant effects of combining NNLO predictions with parton showers are expected in regions where observables are sensitive to soft-gluon radiation.

Figure 7 depicts the transverse-momentum distribution of the hardest jet in the inclusive and the `fiducial-noJV` phase space. The relative behaviour of the results in the two scenarios is very similar. This remains true also for other distributions which is why we refrain from showing any other inclusive result and focus instead only on distributions in

JHEP12(2018)121

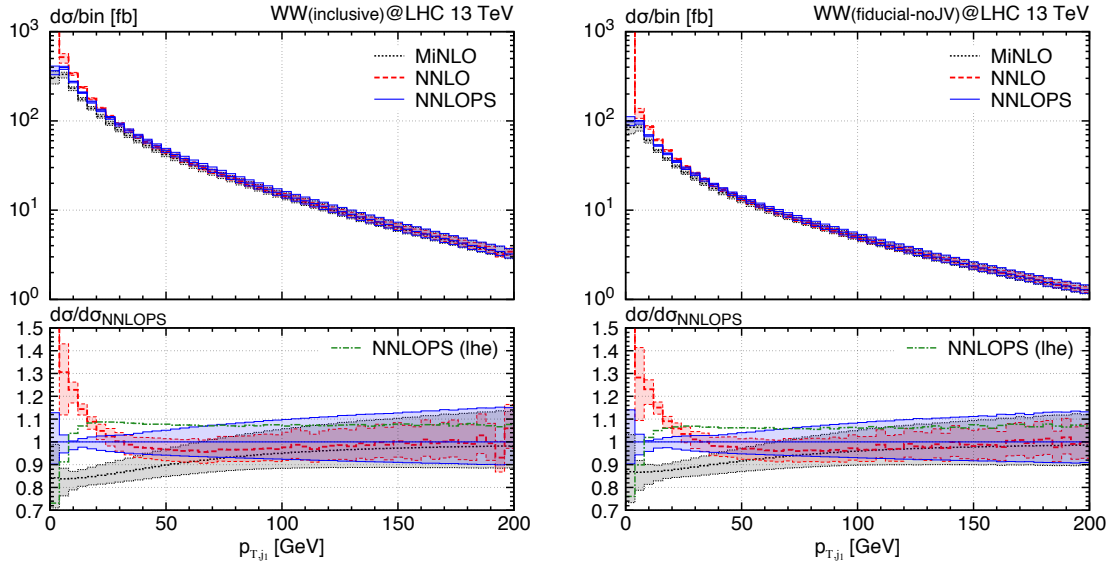

Figure 7. Distribution of the cross section in transverse momentum of the leading jet as predicted by MiNLO (black, dotted), NNLO (red, dashed) and NNLOPS (blue, solid); for reference, central results of NNLOPS at LHE level (green, dash-dotted) are also shown in the ratio frame; (a) inclusive phase space and (b) `fiducial-noJV` setup.

the fiducial phase below. As expected, the NNLO curve diverges as small jet p_T due to large logarithmic terms. On the contrary, both NNLOPS and MiNLO remain finite in the small-p_T region. However, the importance of including NNLO accuracy on top of MiNLO is obvious from the $\sim 15\%$ differences to NNLOPS in that region, which also produce a shape distortion. At high transverse momenta all three predictions have the same (NLO) perturbative accuracy and are consistent within scale uncertainties. The uncertainty band of the NNLOPS result is smallest at around $p_{T,j_1} = 15\,\text{GeV}$. This narrowing of the band is due to the fact that at high p_T the NNLOPS prediction is formally only NLO accurate and at very small p_T the uncertainty increases due to missing large logarithmic higher-order terms. As a consequence, the uncertainty will be smallest in the intermediate-p_T region.

We continue by showing in figure 8 the transverse momentum of the colourless final-state (diboson) system ($p_{T,WW}$).[16] The `fiducial-noJV` setup in the left panel of that figure reveals no surprises: the NNLO curve diverges at small transverse momenta, which is cured in the NNLOPS prediction by the parton shower. The general behaviour is very similar to the p_T distribution of the leading jet. The $p_{T,WW}$ distribution in the `fiducial-JV` setup (right panel of figure 8), on the other hand, shows some quite prominent effects: in the intermediate p_T region ($40\,\text{GeV} \lesssim p_{T,WW} \lesssim 100\,\text{GeV}$) NNLO and NNLOPS results can differ by more than one order of magnitude, while at low p_T NNLO shows the typical unphysical behaviour, and at high p_T the two predictions become similar again. It is

[16] Note that we performed a qualitative comparison of the inclusive $p_{T,WW}$ distribution with the analytically resummed results of refs. [82], and we found remarkable agreement in terms of shape between NNLOPS and NNLL+NNLO.

JHEP12(2018)121

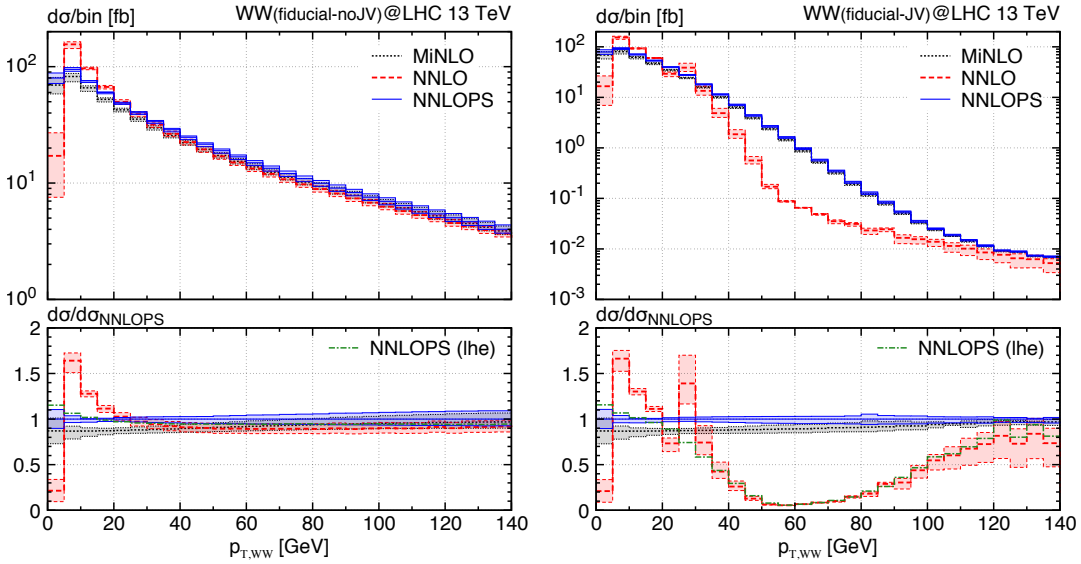

(a) (b)

Figure 8. Same as figure 7, but for the distribution in the transverse momentum of the colourless final-state system; (a) `fiducial-noJV` and (b) `fiducial-JV` phase space.

interesting to notice that the NNLOPS result before showering (see the green, dash-dotted result at LHE level in the ratio) follows closely the NNLO curve in the intermediate p_T range. Hence, this large gap is filled up in the NNLOPS prediction entirely by soft radiation due to the parton shower. This can be understood as follows: beyond the region where jet-veto requirements are applied (25 GeV and 30 GeV respectively) the NNLO $p_{T,WW}$ distribution drops significantly as a substantial fraction of events with a hard jet recoiling against the W^+W^- system is removed. In fact, disregarding high-rapidity jets which escape the jet veto requirements, the NLO distribution has a boundary at the jet veto cut. Thus, the NNLO result is effectively only LO accurate at larger $p_{T,WW}$ values, and only configurations with two jets of transverse momentum less than 25 or 30 GeV can contribute to this region. Eventually, the shower generates additional configurations where three and more jets recoil against the W^+W^- system, so that the intermediate p_T region gets filled up and a smooth and physical distribution is obtained. Since in the intermediate transverse momentum region ($40\,\text{GeV} \lesssim p_{T,WW} \lesssim 100\,\text{GeV}$) the distribution is mainly built up by the colour singlet recoiling against soft jets from the parton shower, in this region the distribution is particularly sensitive to the modeling of soft radiation in the parton shower. Accordingly, this distribution seems particularly suited to tune the parton shower inputs of the NNLOPS generator, both the perturbative components as well as the handling of non-perturbative hadronization effects. Compared to other measurements that enter tunes of parton shower it is interesting to note that the W^+W^- system that is measured is in fact relatively hard. We finally note that the step in the NNLO curve around $p_{T,WW} = 25\,\text{GeV}$ is a perturbative instability from an integrable logarithmic singularity [153] caused by the boundary in the NLO $p_{T,WW}$ distribution due to the jet-veto cut.

Also the distribution in the azimuthal angle between the dilepton system and the missing transverse-momentum vector ($\Delta\phi_{\ell\ell,\nu\nu}$) is sensitive to soft-gluon effects: since the

JHEP12(2018)121

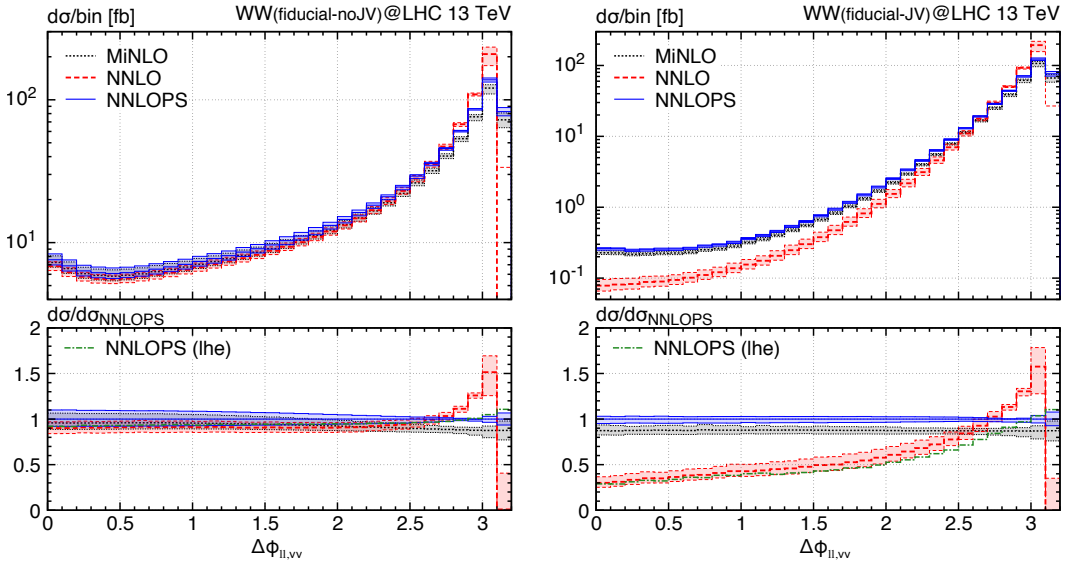

(a) (b)

Figure 9. Same as figure 7, but for the distribution in the azimuthal angle between the dilepton system and the two neutrinos; (a) `fiducial-noJV` and (b) `fiducial-JV` phase space.

two vectors are back-to-back at LO, values different from π are filled only upon inclusion of higher-order corrections. The $\Delta\phi_{\ell\ell,\nu\nu}$ distribution is shown in figure 9 and develops the expected Sudakov-like behaviour at large separation angles. While it is clear that in this region only the showered results provide a proper prediction, at small separation angles MiNLO, NNLO and NNLOPS in the `fiducial-noJV` setup (left panel of that figure) all have the same formal fixed-order accuracy and agree within their respective uncertainty bands. Looking at small $\Delta\phi_{\ell\ell,\nu\nu}$ angles in the setup with a jet-veto (`fiducial-JV`) in the right panel of that figure, on the other hand, we observe a very strong suppression of the NNLO cross section with respect to the NNLOPS one. As in the $p_{T,WW}$ case the green, dash-dotted LHE result in the ratio is very close to NNLO in that region. The explanation follows the same logic as for $p_{T,WW}$ above: the jet-veto suppresses small $\Delta\phi_{\ell\ell,\nu\nu}$ separations as they require the W^+W^- system to recoil against hard jet radiation. The shower reshuffles events such that more of such configurations are generated and increases the cross section at small $\Delta\phi_{\ell\ell,\nu\nu}$. Being dominated by corrections from the shower, also this observable may serve as a way to tune parton showers and as a probe of non-perturbative models in the parton shower Monte Carlo.

To conclude our analysis of differential observables in the fiducial phase, we consider a set of distributions in figure 10 which have been unfolded in the 8 TeV measurement done by ATLAS in ref. [6]. They involve the leading lepton p_T, the transverse momentum, invariant mass and rapidity of the dilepton system, the separation in the azimuthal angle of the two leptons as well as an observable sensitive to new physics searches which is defined through the separation in η of the two leptons:

$$|\cos(\theta^\star)| = |\tanh\left(\Delta\eta_{\ell\ell}/2\right)| \ . \tag{3.5}$$

It is nice to see that, on the one hand, the inclusion of NNLO corrections on top of the

JHEP12(2018)121

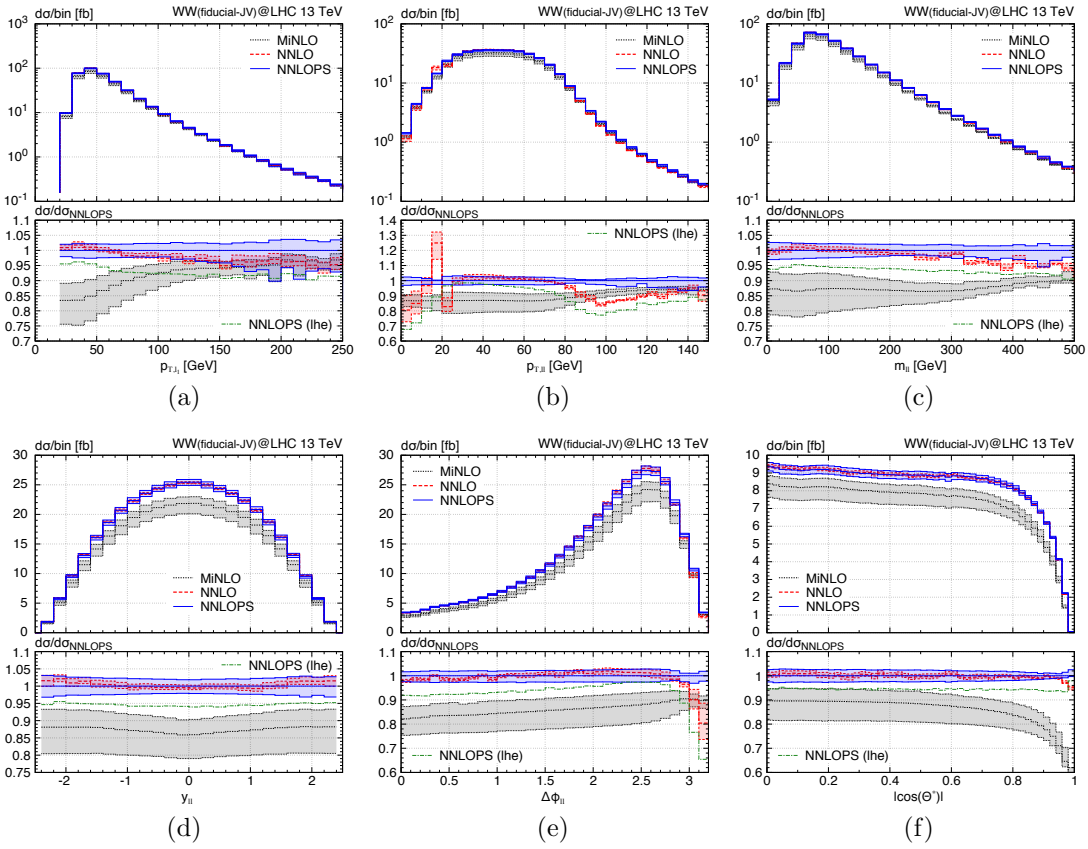

Figure 10. Same as figure 7, but for various distributions in the fiducial phase space measured in the 8 TeV analysis by ATLAS [6]: (a) transverse momentum of the leading lepton p_{T,ℓ_1} (b) transverse momentum $p_{T,\ell\ell}$, (c) invariant mass $m_{\ell^-\ell^+}$ and (d) rapidity of the dilepton pair, (d) azimuthal lepton separation $\Delta\phi_{\ell\ell}$, and (e) $|\cos(\theta^\star)|$ defined in eq. (3.5).

MiNLO generator is crucial not only for the correct normalization, but in many cases also to capture relevant shape effects. On the other hand, the impact of the parton shower on top of the NNLO predictions is moderate in many phase space regions, but absolutely vital in cases where the perturbative prediction fails due to soft radiation effects, as we have already seen in figures 7–9. Moreover, even in some of the distributions where the NNLO prediction is not challenged by large logarithms, the shower induces shape effects at the 5% level, see figure 10 (a) and (c) for example.

The two distribution which require some additional discussion in figure 10 are $p_{T,\ell\ell}$ and $\Delta\phi_{\ell\ell}$. We note at this point that in the fiducial phase space the LHE-level NNLOPS result before shower, which is shown only in the ratio frame, has a different normalization (by about −5%) than after shower. This is due to the jet-veto requirements and does not appear in the inclusive nor the `fiducial-noJV` phase space. It can be understood by realizing that the LHE-level results are unphysical in regions sensitive to soft-gluon radiation where large logarithmic contributions are resummed by the shower. In other phase-space regions LHE-level results coincide with the respective fixed-order result. Since among the fiducial cuts only the jet-veto requirements are subject to effects from soft gluons, large differences

JHEP12(2018)121

between LHE-level and showered results appear in the `fiducial-JV` setup primarily.

The $p_{T,\ell\ell}$ distribution in figure 10 (b) shows some interesting features: at 20 GeV the NNLO curve develops some perturbative instability. The integrable logarithmic singularity [153] is caused by the fiducial $p_T^{\text{miss}} > 20$ GeV cut, which at LO implies that the cross section below $p_{T,\ell\ell} = 20$ GeV vanishes. The reduced formal accuracy of the NNLO calculation in this region is also evident from the larger uncertainty band. As expected, this effect is absent in the NNLOPS result already before the shower. Both the NNLO and the LHE-level NNLOPS curve show a very similar shape at larger $p_{T,\ell\ell}$. Around $p_{T,\ell\ell} = 100$ GeV a dip appears in the ratio to the showered NNLOPS prediction. The reason for this dip is the following: emissions from the parton shower can modify $p_{T,\ell\ell}$ because of recoil effects. Accordingly events can migrate to a different bin. The largest impact of this migration will be right after the point of inflection, which for $p_{T,\ell\ell}$ is at around 100 GeV.

Also for the $\Delta\phi_{\ell\ell}$ distribution in figure 10 (e) the parton shower induces some prominent shape differences in the NNLOPS result. The NNLO and NNLOPS result at LHE level are very similar shape-wise: their curves relative to the NNLOPS one increase slightly with $\Delta\phi_{\ell\ell}$ up to $\Delta\phi_{\ell\ell} \sim 2.5$, after which they drop off significantly towards configurations where the two leptons are back-to-back. This behaviour is caused by the fiducial lepton cuts and is absent in the fully inclusive case. In particular the cut on $p_T^{\text{miss}} > 20$ GeV suppresses the region where the two leptons are back to back in the azimuthal plane. Accordingly, the cross section drops sharply just before $\Delta\phi_{\ell\ell} = \pi$. Because the cross section drops very fast, a small change in $\Delta\phi_{\ell\ell}$ due to the parton shower will have a large effect in the ratio plot. This effect is similar to the one observed around $p_{T,\ell\ell} = 90 - 100$ GeV, see figure 10 (b). In particular the effect of the parton shower is to partially re-populate this region since p_T^{miss} can recoil against extra soft radiation from the parton shower, hence the region close to $\Delta\phi_{\ell\ell} = \pi$ is less suppressed.

In summary, the importance of NNLOPS accurate predictions for W^+W^- production has been demonstrated in the fiducial phase space. Besides IR-sensitive observables which require parton-shower resummation already in the inclusive phase space, also other distributions in the fiducial phase space exhibit sizeable corrections from the parton shower, which cures perturbative instabilities caused by fiducial cuts and provides a more reliable description of jet-veto logarithms present in the fiducial cross section. The relevance of NNLO accuracy beyond the MiNLO description is evident in essentially every observable, irrespective of inclusive or fiducial, integrated or differential.

3.5 Charge asymmetry in W^+W^- production

To complete our presentation of phenomenological results, we turn to discussing the definition of a charge asymmetry in the W^+W^- production process at the LHC. Similar to $t\bar{t}$ production, the two W bosons in W^+W^- production exhibit an asymmetry. This is caused by the fact that W^+W^- is mainly produced through t-channel $u\bar{u}$ or $d\bar{d}$ scattering (s-channel production does not create an asymmetry). Since up quarks in the protons are faster than down quarks and since the W-bosons tend to move in the same direction as the incoming quark, i.e. W^+ (W^-) bosons tend to follow the up (down) quarks, the W^+-bosons tend to be more forward. This asymmetry manifests itself in the rapidity dis-

JHEP12(2018)121

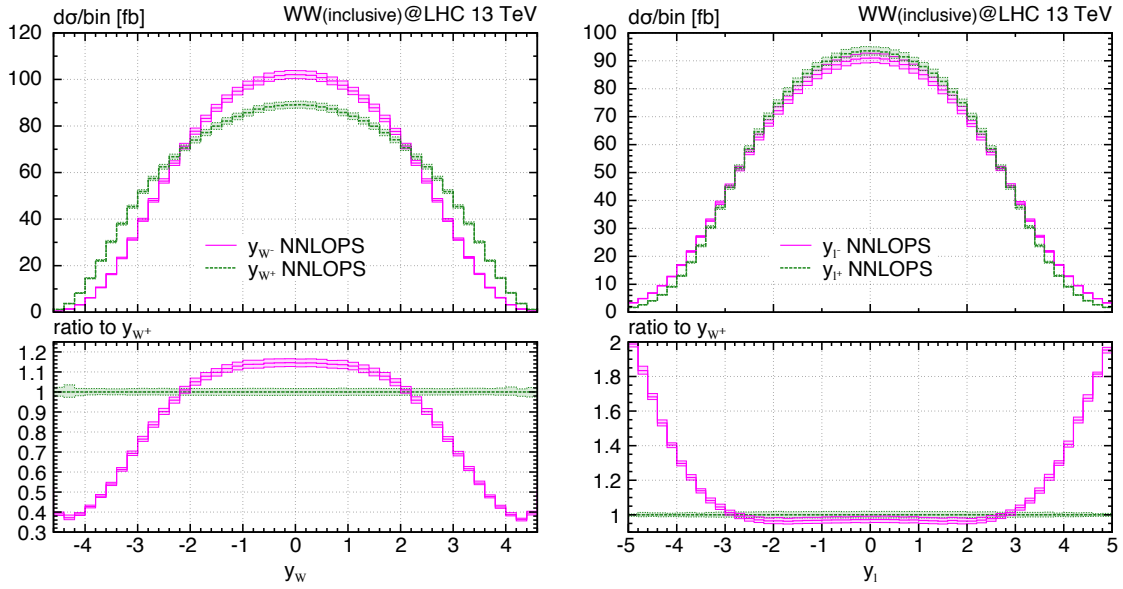

(a) (b)

Figure 11. Comparison of rapidity distributions of negatively (magenta, solid) and positively (green, dotted) charged particles at NNLOPS for (a) the two W bosons and (b) the two leptons.

tributions of the positively and negatively charged W bosons as shown in figure 11 (a): W^+ bosons are generally more forward, while W^- bosons are situated more at central rapidity. However, since the W-boson momenta of the W^+W^- final state are not accessible in the measurement due to the two neutrinos (not even under the assumption that they are on-shell), one may wonder whether this asymmetry persists in the case of the leptons. Indeed, figure 11 (b) shows a similar, but less pronounced behaviour for the leptons. In fact, the asymmetry is reversed with respect to the charges in this case with the ℓ^+ being more central and the ℓ^- more forward.

We can now use the previous observation to define a charge asymmetry in W^+W^- production for the W bosons:

$$A_C^W = \frac{\sigma(|y_{W^+}| > |y_{W^-}|) - \sigma(|y_{W^+}| < |y_{W^-}|)}{\sigma(|y_{W^+}| > |y_{W^-}|) + \sigma(|y_{W^+}| < |y_{W^-}|)}, \tag{3.6}$$

as well as for the leptons:[17]

$$A_C^\ell = \frac{\sigma(|y_{\ell^+}| > |y_{\ell^-}|) - \sigma(|y_{\ell^+}| < |y_{\ell^-}|)}{\sigma(|y_{\ell^+}| > |y_{\ell^-}|) + \sigma(|y_{\ell^+}| < |y_{\ell^-}|)}. \tag{3.7}$$

This allows us to express the size of the asymmetry by a single number. It is zero if there is no asymmetry, positive if the positively-charged particle is more forward, and negative otherwise. Note that the denominator simply corresponds to the integrated cross section, within the considered cuts.

[17]Note that for the leptons, since they are massless, the rapidity entering the asymmetry and the pseudo-rapidity used to define the fiducial cuts coincide ($y_\ell \equiv \eta_\ell$).

JHEP12(2018)121

NNLOPS	inclusive phase space	fiducial phase space
A_C^W	$0.1263(1)^{+2.1\%}_{-1.8\%}$	$0.0726(3)^{+2.0\%}_{-2.6\%}$
A_C^ℓ	$-\left[0.0270(1)^{+5.0\%}_{-6.4\%}\right]$	$-\left[0.0009(4)^{+72\%}_{-87\%}\right]$

Table 3. NNLOPS predictions for the charge asymmetry for W-bosons and charged leptons in W^+W^- production. The fiducial volume is defined in table 1 (including the jet-veto requirement).

Table 3 summarizes the NNLOPS predictions for A_C^W and A_C^ℓ in the inclusive and in the fiducial phase. The uncertainties are obtained by computing a 7-point variation in the numerator and dividing by the central cross section in the denominator. This choice is motivated by the fact that fully correlated uncertainties in the ratio lead to too small uncertainties for A_C^W. The W-boson asymmetry in the inclusive phase space is pretty large and positive, as one could expect from figure 11 (a). It is significantly reduced by the fiducial cuts, but still clearly different from zero. Also the leptons yield a charge asymmetry at inclusive level, which, however, is smaller than for W bosons and negative. Unfortunately, once lepton cuts are applied in the fiducial volume A_C^ℓ becomes almost compatible with zero within both perturbative and numerical uncertainties. This again is due to the left-handed nature of the W-boson interactions: in the case of the W^+ decay, the neutrino tends to follow the W direction while the positive charged lepton will mostly end up in the central region of the detector. When the W^- decays, it is instead the negative charged lepton that tends to follow the W boson in the forward region, while the neutrino ends up in the central region of the detector compared to the W boson rapidity. This effect ends up fully compensating the W-boson charge asymmetry and even causing the leptons to have an asymmetry that is reversed in sign. The relative importance of these two effects depends on kinematics of the leptons and can then be altered by probing different kinematic regions. For instance, it is clear from the plots that by widening the rapidity requirements on the leptons and measureing them further into the forward region (beyond $|\eta_\ell| = 2.4$) a non-zero charge asymmetry could be measured by the experiments. It would be interesting to see whether such measurement can be performed at LHCb, which already measured a lepton charge asymmetry in Drell-Yan production [154]. Furthermore, we verified explicitly that the lepton asymmetry increases when going to a boosted regime of the W bosons, due to its sensitivity to the W-boson polarizations. In this region, BSM effects that alter the W-polarization composition could considerably modify the value of A_C^ℓ, so that the lepton asymmetry can be used as a probe of new physics. A more detailed analysis of such effects is, however, beyond the scope of the present paper.

4 Summary

In this paper we presented NNLO-accurate parton-shower predictions for the production of W^+W^- pairs at hadron colliders. We include off-shell effects and spin correlations by considering the full leptonic process with two charged leptons and the two corresponding neutrinos in the final state ($\ell\nu_\ell\ell'\nu_{\ell'}$). For the first time NNLO QCD corrections have been

JHEP12(2018)121

consistently matched to parton showers for a $2 \to 4$ process. Our calculation has been extensively validated by the excellent agreement of the NNLOPS Les Houches events with NNLO predictions for Born-level observables.

We have studied the impact of including NNLO corrections on top of the MiNLO generator and of including the parton shower on top of NNLO predictions on rates and distributions in both inclusive and fiducial phase spaces. Integrated cross sections predicted by our NNLOPS computation are virtually identical with the NNLO cross section and in good agreement with cross-section measurements for W^+W^- production by ATLAS and CMS. The relevance of the parton shower to resum jet-veto logarithms beyond the ones present at NNLO is moderate: down to jet-veto cuts of 15 GeV NNLO agrees with NNLOPS to better than about 2%, but becomes unreliable below such values.

The importance of NNLOPS predictions compared to fixed order becomes most apparent in differential distributions which are sensitive to soft-gluon effects. In these phase-space regions the validity of QCD perturbation theory breaks down due to the presence of large logarithmic contributions, but matching to the parton shower recovers physical predictions by the NNLOPS computation for all observables. Even observables which develop no logarithmic divergences at inclusive level can feature perturbative instabilities as soon as fiducial cuts are applied. Hence, also in such cases NNLOPS matching can induce substantial effects beyond NNLO as far as distributions in the fiducial phase space are concerned. Several examples have been presented where fiducial cuts, primarily the jet-veto requirements, but also lepton cuts, challenge fixed order predictions and cause an improved description by NNLOPS. Moreover, we found NNLO-corrections to have a significant impact beyond the MiNLO computation throughout: by and large NNLOPS and MiNLO show differences at the 10%-level and higher.

We reckon that the NNLOPS calculation and the results presented in this paper will be highly valuable for experimental measurements, which feature W^+W^- final states as signal or background. The computation is publicly available within the POWHEG BOX framework and allows for fully-exclusive hadron-level event generation, which can be combined by the experiments with their detector simulation.

Acknowledgments

We thank Fabrizio Caola, Massimiliano Grazzini, Uli Haisch, Keith Hamilton, Stefan Kallweit, Pier Francesco Monni, Paolo Nason and Andrea Wulzer for many stimulating and helpful discussions. We are grateful to Kristin Lohwasser, Philip Sommer and Jochen Meyer for discussion on the experimental setup and details of the measurements. We are also indebted to Massimiliano Grazzini, Keith Hamilton and Pier Francesco Monni for comments on the manuscript. This work was supported in part by ERC Consolidator Grant HICCUP (No. 614577). The work of ER is supported by a Marie Skłodowska-Curie Individual Fellowship of the European Commission's Horizon 2020 Programme under contract number 659147 PrecisionTools4LHC.

Open Access. This article is distributed under the terms of the Creative Commons Attribution License (CC-BY 4.0), which permits any use, distribution and reproduction in any medium, provided the original author(s) and source are credited.

JHEP12(2018)121

References

[1] CDF collaboration, T. Aaltonen et al., *Measurement of the W^+W^- production cross section and search for anomalous $WW\gamma$ and WWZ couplings in $p\bar{p}$ collisions at $\sqrt{s} = 1.96$ TeV*, *Phys. Rev. Lett.* **104** (2010) 201801 [arXiv:0912.4500] [INSPIRE].

[2] D0 collaboration, V.M. Abazov et al., *Measurements of WW and WZ production in W + jets final states in $p\bar{p}$ collisions*, *Phys. Rev. Lett.* **108** (2012) 181803 [arXiv:1112.0536] [INSPIRE].

[3] ATLAS collaboration, *Measurement of W^+W^- production in pp collisions at $\sqrt{s} = 7$ TeV with the ATLAS detector and limits on anomalous WWZ and $WW\gamma$ couplings*, *Phys. Rev.* **D 87** (2013) 112001 [*Erratum ibid.* **D 88** (2013) 079906] [arXiv:1210.2979] [INSPIRE].

[4] CMS collaboration, *Measurement of the W^+W^- cross section in pp collisions at $\sqrt{s} = 7$ TeV and limits on anomalous $WW\gamma$ and WWZ couplings*, *Eur. Phys. J.* **C 73** (2013) 2610 [arXiv:1306.1126] [INSPIRE].

[5] ATLAS collaboration, *Measurement of the W^+W^- production cross section in proton-proton collisions at $\sqrt{s} = 8$ TeV with the ATLAS detector*, ATLAS-CONF-2014-033 (2014).

[6] ATLAS collaboration, *Measurement of total and differential W^+W^- production cross sections in proton-proton collisions at $\sqrt{s} = 8$ TeV with the ATLAS detector and limits on anomalous triple-gauge-boson couplings*, *JHEP* **09** (2016) 029 [arXiv:1603.01702] [INSPIRE].

[7] CMS collaboration, *Measurement of W^+W^- and ZZ production cross sections in pp collisions at $\sqrt{s} = 8$ TeV*, *Phys. Lett.* **B 721** (2013) 190 [arXiv:1301.4698] [INSPIRE].

[8] CMS collaboration, *Measurement of the W^+W^- cross section in pp collisions at $\sqrt{s} = 8$ TeV and limits on anomalous gauge couplings*, *Eur. Phys. J.* **C 76** (2016) 401 [arXiv:1507.03268] [INSPIRE].

[9] ATLAS collaboration, *Measurement of the W^+W^- production cross section in pp collisions at a centre-of-mass energy of $\sqrt{s} = 13$ TeV with the ATLAS experiment*, *Phys. Lett.* **B 773** (2017) 354 [arXiv:1702.04519] [INSPIRE].

[10] ucms Collaboration, *Measurement of the WW cross section pp collisions at $\sqrt{s}$=13 TeV*, CMS-PAS-SMP-16-006 (2016).

[11] ATLAS, CDF, CMS, D0 collaboration, *Diboson Production at LHC and Tevatron*, *Int. J. Mod. Phys. Conf. Ser.* **31** (2014) 1460279 [arXiv:1403.1415] [INSPIRE].

[12] C. Frye, M. Freytsis, J. Scholtz and M.J. Strassler, *Precision diboson observables for the LHC*, *JHEP* **03** (2016) 171 [arXiv:1510.08451] [INSPIRE].

[13] A. Butter et al., *The gauge-Higgs legacy of the LHC run I*, *JHEP* **07** (2016) 152 [arXiv:1604.03105] [INSPIRE].

[14] Z. Zhang, *Time to go beyond triple-gauge-boson-coupling interpretation of W pair production*, *Phys. Rev. Lett.* **118** (2017) 011803 [arXiv:1610.01618] [INSPIRE].

[15] D.R. Green, P. Meade and M.-A. Pleier, *Multiboson interactions at the LHC*, *Rev. Mod. Phys.* **89** (2017) 035008 [arXiv:1610.07572] [INSPIRE].

[16] J. Baglio, S. Dawson and I.M. Lewis, *An NLO QCD effective field theory analysis of W^+W^- production at the LHC including fermionic operators*, *Phys. Rev.* **D 96** (2017) 073003 [arXiv:1708.03332] [INSPIRE].

JHEP12(2018)121

[17] A. Falkowski et al., *Anomalous triple gauge couplings in the effective field theory approach at the LHC*, *JHEP* **02** (2017) 115 [arXiv:1609.06312] [INSPIRE].

[18] G. Panico, F. Riva and A. Wulzer, *Diboson Interference Resurrection*, *Phys. Lett.* **B 776** (2018) 473 [arXiv:1708.07823] [INSPIRE].

[19] R. Franceschini et al., *Electroweak Precision Tests in High-Energy Diboson Processes*, *JHEP* **02** (2018) 111 [arXiv:1712.01310] [INSPIRE].

[20] D. Liu and L.-T. Wang, *Precision measurement with diboson at the LHC*, arXiv:1804.08688 [INSPIRE].

[21] ATLAS collaboration, *Observation of a new particle in the search for the standard model Higgs boson with the ATLAS detector at the LHC*, *Phys. Lett.* **B 716** (2012) 1 [arXiv:1207.7214] [INSPIRE].

[22] ATLAS collaboration, *Observation and measurement of Higgs boson decays to WW^* with the ATLAS detector*, *Phys. Rev.* **D 92** (2015) 012006 [arXiv:1412.2641] [INSPIRE].

[23] ATLAS collaboration, *Measurement of fiducial differential cross sections of gluon-fusion production of Higgs bosons decaying to $WW^* \to e\nu\mu\nu$ with the ATLAS detector at $\sqrt{s} = 8$ TeV*, *JHEP* **08** (2016) 104 [arXiv:1604.02997] [INSPIRE].

[24] CMS collaboration, *Observation of a new boson at a mass of 125 GeV with the CMS experiment at the LHC*, *Phys. Lett.* **B 716** (2012) 30 [arXiv:1207.7235] [INSPIRE].

[25] CMS collaboration, *Observation of a new boson with mass near 125 GeV in pp collisions at $\sqrt{s} = 7$ and 8 TeV*, *JHEP* **06** (2013) 081 [arXiv:1303.4571] [INSPIRE].

[26] CMS collaboration, *Measurement of Higgs boson production and properties in the WW decay channel with leptonic final states*, *JHEP* **01** (2014) 096 [arXiv:1312.1129] [INSPIRE].

[27] ATLAS collaboration, *Study of the spin and parity of the Higgs boson in diboson decays with the ATLAS detector*, *Eur. Phys. J.* **C 75** (2015) 476 [*Erratum ibid.* **C 76** (2016) 152] [arXiv:1506.05669] [INSPIRE].

[28] CMS collaboration, *Measurement of the transverse momentum spectrum of the Higgs boson produced in pp collisions at $\sqrt{s} = 8$ TeV using $H \to WW$ decays*, *JHEP* **03** (2017) 032 [arXiv:1606.01522] [INSPIRE].

[29] R.W. Brown and K.O. Mikaelian, *W^+W^- and Z^0Z^0 pair production in $e^+e^-, pp, p\bar{p}$ colliding beams*, *Phys. Rev.* **D 19** (1979) 922 [INSPIRE].

[30] J. Ohnemus, *An order α^-s calculation of hadronic W^-W^+ production*, *Phys. Rev.* **D 44** (1991) 1403 [INSPIRE].

[31] S. Frixione, *A next-to-leading order calculation of the cross-section for the production of W^+W^- pairs in hadronic collisions*, *Nucl. Phys.* **B 410** (1993) 280 [INSPIRE].

[32] J.M. Campbell and R.K. Ellis, *An update on vector boson pair production at hadron colliders*, *Phys. Rev.* **D 60** (1999) 113006 [hep-ph/9905386] [INSPIRE].

[33] L.J. Dixon, Z. Kunszt and A. Signer, *Vector boson pair production in hadronic collisions at order α_s: lepton correlations and anomalous couplings*, *Phys. Rev.* **D 60** (1999) 114037 [hep-ph/9907305] [INSPIRE].

[34] L.J. Dixon, Z. Kunszt and A. Signer, *Helicity amplitudes for $O(\alpha_s)$ production of W^+W^-, $W^\pm Z$, ZZ, $W^\pm\gamma$, or $Z\gamma$ pairs at hadron colliders*, *Nucl. Phys.* **B 531** (1998) 3 [hep-ph/9803250] [INSPIRE].

[35] J.M. Campbell, R.K. Ellis and C. Williams, *Vector boson pair production at the LHC*, *JHEP* **07** (2011) 018 [arXiv:1105.0020] [INSPIRE].

JHEP12(2018)121

[36] A. Bierweiler, T. Kasprzik, J.H. Kühn and S. Uccirati, *Electroweak corrections to W-boson pair production at the LHC*, *JHEP* **11** (2012) 093 [arXiv:1208.3147] [INSPIRE].

[37] J. Baglio, L.D. Ninh and M.M. Weber, *Massive gauge boson pair production at the LHC: a next-to-leading order story*, *Phys. Rev.* **D 88** (2013) 113005 [*Erratum ibid.* **D 94** (2016) 099902] [arXiv:1307.4331] [INSPIRE].

[38] M. Billóni, S. Dittmaier, B. Jäger and C. Speckner, *Next-to-leading order electroweak corrections to $pp \to W^+W^- \to 4$ leptons at the LHC in double-pole approximation*, *JHEP* **12** (2013) 043 [arXiv:1310.1564] [INSPIRE].

[39] B. Biedermann et al., *Next-to-leading-order electroweak corrections to $pp \to W^+W^- \to 4$ leptons at the LHC*, *JHEP* **06** (2016) 065 [arXiv:1605.03419] [INSPIRE].

[40] S. Dittmaier, S. Kallweit and P. Uwer, *NLO QCD corrections to WW+jet production at hadron colliders*, *Phys. Rev. Lett.* **100** (2008) 062003 [arXiv:0710.1577] [INSPIRE].

[41] J.M. Campbell, R.K. Ellis and G. Zanderighi, *Next-to-leading order predictions for $WW + 1$ jet distributions at the LHC*, *JHEP* **12** (2007) 056 [arXiv:0710.1832] [INSPIRE].

[42] S. Dittmaier, S. Kallweit and P. Uwer, *NLO QCD corrections to $pp/p\bar{p} \to WW$ + jet + X including leptonic W-boson decays*, *Nucl. Phys.* **B 826** (2010) 18 [arXiv:0908.4124] [INSPIRE].

[43] J.M. Campbell, D.J. Miller and T. Robens, *Next-to-Leading order predictions for WW + jet production*, *Phys. Rev.* **D 92** (2015) 014033 [arXiv:1506.04801] [INSPIRE].

[44] T. Melia, K. Melnikov, R. Rontsch and G. Zanderighi, *NLO QCD corrections for W^+W^- pair production in association with two jets at hadron colliders*, *Phys. Rev.* **D 83** (2011) 114043 [arXiv:1104.2327] [INSPIRE].

[45] N. Greiner et al., *NLO QCD corrections to the production of W^+W^- plus two jets at the LHC*, *Phys. Lett.* **B 713** (2012) 277 [arXiv:1202.6004] [INSPIRE].

[46] F. Febres Cordero, P. Hofmann and H. Ita, *W^+W^- + 3-jet production at the large hadron collider in next-to-leading-order QCD*, *Phys. Rev.* **D 95** (2017) 034006 [arXiv:1512.07591] [INSPIRE].

[47] D.A. Dicus, C. Kao and W.W. Repko, *Gluon production of gauge bosons*, *Phys. Rev.* **D 36** (1987) 1570 [INSPIRE].

[48] E.W.N. Glover and J.J. van der Bij, *Vector boson pair production via gluon fusion*, *Phys. Lett.* **B 219** (1989) 488 [INSPIRE].

[49] T. Binoth, M. Ciccolini, N. Kauer and M. Krämer, *Gluon-induced WW background to Higgs boson searches at the LHC*, *JHEP* **03** (2005) 065 [hep-ph/0503094] [INSPIRE].

[50] T. Binoth, M. Ciccolini, N. Kauer and M. Krämer, *Gluon-induced W-boson pair production at the LHC*, *JHEP* **12** (2006) 046 [hep-ph/0611170] [INSPIRE].

[51] J.M. Campbell, R.K. Ellis and C. Williams, *Gluon-gluon contributions to W^+W^- production and Higgs interference effects*, *JHEP* **10** (2011) 005 [arXiv:1107.5569] [INSPIRE].

[52] T. Melia, K. Melnikov, R. Rontsch, M. Schulze and G. Zanderighi, *Gluon fusion contribution to W^+W^- + jet production*, *JHEP* **08** (2012) 115 [arXiv:1205.6987] [INSPIRE].

[53] F. Caola et al., *Two-loop helicity amplitudes for the production of two off-shell electroweak bosons in gluon fusion*, *JHEP* **06** (2015) 129 [arXiv:1503.08759] [INSPIRE].

[54] A. von Manteuffel and L. Tancredi, *The two-loop helicity amplitudes for $gg \to V_1V_2 \to 4$ leptons*, *JHEP* **06** (2015) 197 [arXiv:1503.08835] [INSPIRE].

JHEP12(2018)121

[55] F. Caola, K. Melnikov, R. Röntsch and L. Tancredi, *QCD corrections to W^+W^- production through gluon fusion*, *Phys. Lett.* **B 754** (2016) 275 [arXiv:1511.08617] [INSPIRE].

[56] F. Caola et al., *QCD corrections to vector boson pair production in gluon fusion including interference effects with off-shell Higgs at the LHC*, *JHEP* **07** (2016) 087 [arXiv:1605.04610] [INSPIRE].

[57] T. Gehrmann et al., *W^+W^- production at hadron colliders in next to next to leading order QCD*, *Phys. Rev. Lett.* **113** (2014) 212001 [arXiv:1408.5243] [INSPIRE].

[58] M. Grazzini, S. Kallweit, S. Pozzorini, D. Rathlev and M. Wiesemann, *W^+W^- production at the LHC: fiducial cross sections and distributions in NNLO QCD*, *JHEP* **08** (2016) 140 [arXiv:1605.02716] [INSPIRE].

[59] T. Gehrmann, A. von Manteuffel, L. Tancredi and E. Weihs, *The two-loop master integrals for $q\bar{q} \to VV$*, *JHEP* **06** (2014) 032 [arXiv:1404.4853] [INSPIRE].

[60] F. Caola et al., *Two-loop helicity amplitudes for the production of two off-shell electroweak bosons in quark-antiquark collisions*, *JHEP* **11** (2014) 041 [arXiv:1408.6409] [INSPIRE].

[61] T. Gehrmann, A. von Manteuffel and L. Tancredi, *The two-loop helicity amplitudes for $q\bar{q}' \to V_1V_2 \to 4$ leptons*, *JHEP* **09** (2015) 128 [arXiv:1503.04812] [INSPIRE].

[62] S. Frixione and B.R. Webber, *Matching NLO QCD computations and parton shower simulations*, *JHEP* **06** (2002) 029 [hep-ph/0204244] [INSPIRE].

[63] K. Hamilton, *A positive-weight next-to-leading order simulation of weak boson pair production*, *JHEP* **01** (2011) 009 [arXiv:1009.5391] [INSPIRE].

[64] S. Hoche, F. Krauss, M. Schonherr and F. Siegert, *Automating the POWHEG method in Sherpa*, *JHEP* **04** (2011) 024 [arXiv:1008.5399] [INSPIRE].

[65] T. Melia, P. Nason, R. Rontsch and G. Zanderighi, *W^+W^-, WZ and ZZ production in the POWHEG BOX*, *JHEP* **11** (2011) 078 [arXiv:1107.5051] [INSPIRE].

[66] P. Nason and G. Zanderighi, *W^+W^- , WZ and ZZ production in the POWHEG-BOX-V2*, *Eur. Phys. J.* **C 74** (2014) 2702 [arXiv:1311.1365] [INSPIRE].

[67] J. Bellm et al., *Anomalous coupling, top-mass and parton-shower effects in W^+W^- production*, *JHEP* **05** (2016) 106 [arXiv:1602.05141] [INSPIRE].

[68] J. Bellm et al., *HERWIG 7.0/HERWIG++ 3.0 release note*, *Eur. Phys. J.* **C 76** (2016) 196 [arXiv:1512.01178] [INSPIRE].

[69] F. Campanario, M. Rauch and S. Sapeta, *W^+W^- production at high transverse momenta beyond NLO*, *Nucl. Phys.* **B 879** (2014) 65 [arXiv:1309.7293] [INSPIRE].

[70] T. Gehrmann, S. Hoche, F. Krauss, M. Schonherr and F. Siegert, *NLO QCD matrix elements + parton showers in $e^+e^- \to$ hadrons*, *JHEP* **01** (2013) 144 [arXiv:1207.5031] [INSPIRE].

[71] S. Hoeche, F. Krauss, M. Schonherr and F. Siegert, *QCD matrix elements + parton showers: the NLO case*, *JHEP* **04** (2013) 027 [arXiv:1207.5030] [INSPIRE].

[72] F. Cascioli et al., *Precise Higgs-background predictions: merging NLO QCD and squared quark-loop corrections to four-lepton + 0,1 jet production*, *JHEP* **01** (2014) 046 [arXiv:1309.0500] [INSPIRE].

[73] R. Frederix and S. Frixione, *Merging meets matching in MC@NLO*, *JHEP* **12** (2012) 061 [arXiv:1209.6215] [INSPIRE].

JHEP12(2018)121

[74] J. Alwall et al., *The automated computation of tree-level and next-to-leading order differential cross sections and their matching to parton shower simulations*, *JHEP* **07** (2014) 079 [arXiv:1405.0301] [INSPIRE].

[75] K. Hamilton, P. Nason and G. Zanderighi, *MINLO: multi-scale improved NLO*, *JHEP* **10** (2012) 155 [arXiv:1206.3572] [INSPIRE].

[76] K. Hamilton, P. Nason, C. Oleari and G. Zanderighi, *Merging $H/W/Z + 0$ and 1 jet at NLO with no merging scale: a path to parton shower + NNLO matching*, *JHEP* **05** (2013) 082 [arXiv:1212.4504] [INSPIRE].

[77] P. Nason, *A New method for combining NLO QCD with shower Monte Carlo algorithms*, *JHEP* **11** (2004) 040 [hep-ph/0409146] [INSPIRE].

[78] S. Frixione, P. Nason and C. Oleari, *Matching NLO QCD computations with Parton Shower simulations: the POWHEG method*, *JHEP* **11** (2007) 070 [arXiv:0709.2092] [INSPIRE].

[79] S. Alioli, P. Nason, C. Oleari and E. Re, *A general framework for implementing NLO calculations in shower Monte Carlo programs: the POWHEG BOX*, *JHEP* **06** (2010) 043 [arXiv:1002.2581] [INSPIRE].

[80] K. Hamilton, T. Melia, P.F. Monni, E. Re and G. Zanderighi, *Merging WW and WW + jet with MINLO*, *JHEP* **09** (2016) 057 [arXiv:1606.07062] [INSPIRE].

[81] S. Dawson, I.M. Lewis and M. Zeng, *Threshold resummed and approximate next-to-next-to-leading order results for W^+W^- pair production at the LHC*, *Phys. Rev.* **D 88** (2013) 054028 [arXiv:1307.3249] [INSPIRE].

[82] M. Grazzini, S. Kallweit, D. Rathlev and M. Wiesemann, *Transverse-momentum resummation for vector-boson pair production at NNLL+NNLO*, *JHEP* **08** (2015) 154 [arXiv:1507.02565] [INSPIRE].

[83] S. Dawson, P. Jaiswal, Y. Li, H. Ramani and M. Zeng, *Resummation of jet veto logarithms at N^3LL_a + NNLO for W^+W^- production at the LHC*, *Phys. Rev.* **D 94** (2016) 114014 [arXiv:1606.01034] [INSPIRE].

[84] M. Grazzini, *Soft-gluon effects in WW production at hadron colliders*, *JHEP* **01** (2006) 095 [hep-ph/0510337] [INSPIRE].

[85] Y. Wang et al., *Transverse-momentum resummation for gauge boson pair production at the hadron collider*, *Phys. Rev.* **D 88** (2013) 114017 [arXiv:1307.7520] [INSPIRE].

[86] P. Meade, H. Ramani and M. Zeng, *Transverse momentum resummation effects in W^+W^- measurements*, *Phys. Rev.* **D 90** (2014) 114006 [arXiv:1407.4481] [INSPIRE].

[87] P. Jaiswal and T. Okui, *Explanation of the WW excess at the LHC by jet-veto resummation*, *Phys. Rev.* **D 90** (2014) 073009 [arXiv:1407.4537] [INSPIRE].

[88] T. Becher, R. Frederix, M. Neubert and L. Rothen, *Automated NNLL + NLO resummation for jet-veto cross sections*, *Eur. Phys. J.* **C 75** (2015) 154 [arXiv:1412.8408] [INSPIRE].

[89] P.F. Monni and G. Zanderighi, *On the excess in the inclusive $W^+W^- \to l^+l^-\nu\overline{\nu}$ cross section*, *JHEP* **05** (2015) 013 [arXiv:1410.4745] [INSPIRE].

[90] M. Grazzini, S. Kallweit and M. Wiesemann, *Fully differential NNLO computations with MATRIX*, *Eur. Phys. J.* **C 78** (2018) 537 [arXiv:1711.06631] [INSPIRE].

[91] M. Grazzini, S. Kallweit, M. Wiesemann *Matrix: "*MUNICH *Automates qT subtraction and Resummation to Integrate X-sections*, http://matrix.hepforge.org/.

[92] K. Hamilton, P. Nason, E. Re and G. Zanderighi, *NNLOPS simulation of Higgs boson production*, *JHEP* **10** (2013) 222 [arXiv:1309.0017] [INSPIRE].

JHEP12(2018)121

[93] K. Hamilton, P. Nason and G. Zanderighi, *Finite quark-mass effects in the NNLOPS POWHEG+MiNLO Higgs generator*, *JHEP* **05** (2015) 140 [arXiv:1501.04637] [INSPIRE].

[94] A. Karlberg, E. Re and G. Zanderighi, *NNLOPS accurate Drell-Yan production*, *JHEP* **09** (2014) 134 [arXiv:1407.2940] [INSPIRE].

[95] W. Astill, W. Bizon, E. Re and G. Zanderighi, *NNLOPS accurate associated HW production*, *JHEP* **06** (2016) 154 [arXiv:1603.01620] [INSPIRE].

[96] J.C. Collins and D.E. Soper, *Angular distribution of dileptons in high-energy hadron collisions*, *Phys. Rev.* **D 16** (1977) 2219 [INSPIRE].

[97] N. Kauer and G. Passarino, *Inadequacy of zero-width approximation for a light Higgs boson signal*, *JHEP* **08** (2012) 116 [arXiv:1206.4803] [INSPIRE].

[98] S. Alioli, F. Caola, G. Luisoni and R. Röntsch, *ZZ production in gluon fusion at NLO matched to parton-shower*, *Phys. Rev.* **D 95** (2017) 034042 [arXiv:1609.09719] [INSPIRE].

[99] S. Kallweit, J.M. Lindert, S. Pozzorini and M. Schönherr, *NLO QCD+EW predictions for $2\ell 2\nu$ diboson signatures at the LHC*, *JHEP* **11** (2017) 120 [arXiv:1705.00598] [INSPIRE].

[100] M. Grazzini, S. Kallweit, D. Rathlev and A. Torre, *$Z\gamma$ production at hadron colliders in NNLO QCD*, *Phys. Lett.* **B 731** (2014) 204 [arXiv:1309.7000] [INSPIRE].

[101] M. Grazzini, S. Kallweit and D. Rathlev, *$W\gamma$ and $Z\gamma$ production at the LHC in NNLO QCD*, *JHEP* **07** (2015) 085 [arXiv:1504.01330] [INSPIRE].

[102] F. Cascioli et al., *ZZ production at hadron colliders in NNLO QCD*, *Phys. Lett.* **B 735** (2014) 311 [arXiv:1405.2219] [INSPIRE].

[103] M. Grazzini, S. Kallweit and D. Rathlev, *ZZ production at the LHC: fiducial cross sections and distributions in NNLO QCD*, *Phys. Lett.* **B 750** (2015) 407 [arXiv:1507.06257] [INSPIRE].

[104] M. Grazzini, S. Kallweit, D. Rathlev and M. Wiesemann, *$W^{\pm}Z$ production at hadron colliders in NNLO QCD*, *Phys. Lett.* **B 761** (2016) 179 [arXiv:1604.08576] [INSPIRE].

[105] M. Grazzini, S. Kallweit, D. Rathlev and M. Wiesemann, *$W^{\pm}Z$ production at the LHC: fiducial cross sections and distributions in NNLO QCD*, *JHEP* **05** (2017) 139 [arXiv:1703.09065] [INSPIRE].

[106] D. de Florian et al., *Differential Higgs boson pair production at next-to-next-to-leading order in QCD*, *JHEP* **09** (2016) 151 [arXiv:1606.09519] [INSPIRE].

[107] M. Grazzini et al., *Higgs boson pair production at NNLO with top quark mass effects*, *JHEP* **05** (2018) 059 [arXiv:1803.02463] [INSPIRE].

[108] S. Catani and M. Grazzini, *An NNLO subtraction formalism in hadron collisions and its application to Higgs boson production at the LHC*, *Phys. Rev. Lett.* **98** (2007) 222002 [hep-ph/0703012] [INSPIRE].

[109] S. Catani and M.H. Seymour, *The dipole formalism for the calculation of QCD jet cross-sections at next-to-leading order*, *Phys. Lett.* **B 378** (1996) 287 [hep-ph/9602277] [INSPIRE].

[110] S. Catani and M.H. Seymour, *A general algorithm for calculating jet cross-sections in NLO QCD*, *Nucl. Phys.* **B 485** (1997) 291 [*Erratum ibid.* **B 510** (1998) 503] [hep-ph/9605323] [INSPIRE].

[111] S. Kallweit et al., *NLO electroweak automation and precise predictions for W+multijet production at the LHC*, *JHEP* **04** (2015) 012 [arXiv:1412.5157] [INSPIRE].

JHEP12(2018)121

[112] S. Kallweit et al., *NLO QCD+EW predictions for V + jets including off-shell vector-boson decays and multijet merging*, *JHEP* **04** (2016) 021 [arXiv:1511.08692] [INSPIRE].

[113] S. Kallweit, *Munich: MUlti-chaNnel Integrator at Swiss (CH) precision —An automated parton level NLO generator*.

[114] A. Denner, S. Dittmaier and L. Hofer, *COLLIER — A Fortran-library for one-loop integrals*, PoS(LL2014)071 [arXiv:1407.0087] [INSPIRE].

[115] A. Denner, S. Dittmaier and L. Hofer, *Collier: a Fortran-based Complex One-Loop library in Extended Regularizations*, *Comput. Phys. Commun.* **212** (2017) 220 [arXiv:1604.06792] [INSPIRE].

[116] G. Ossola, C.G. Papadopoulos and R. Pittau, *CutTools: a program implementing the OPP reduction method to compute one-loop amplitudes*, *JHEP* **03** (2008) 042 [arXiv:0711.3596] [INSPIRE].

[117] A. van Hameren, *OneLOop: for the evaluation of one-loop scalar functions*, *Comput. Phys. Commun.* **182** (2011) 2427 [arXiv:1007.4716] [INSPIRE].

[118] F. Cascioli, P. Maierhofer and S. Pozzorini, *Scattering amplitudes with open loops*, *Phys. Rev. Lett.* **108** (2012) 111601 [arXiv:1111.5206] [INSPIRE].

[119] F. Buccioni, S. Pozzorini and M. Zoller, *On-the-fly reduction of open loops*, *Eur. Phys. J.* **C 78** (2018) 70 [arXiv:1710.11452] [INSPIRE].

[120] F. Cascioli, J. Lindert, P. Maierhöfer and S. Pozzorini, *The OpenLoops one-loop generator*, http://openloops.hepforge.org.

[121] C. Anastasiou, E.W.N. Glover and M.E. Tejeda-Yeomans, *Two loop QED and QCD corrections to massless fermion boson scattering*, *Nucl. Phys.* **B 629** (2002) 255 [hep-ph/0201274] [INSPIRE].

[122] T. Gehrmann and L. Tancredi, *Two-loop QCD helicity amplitudes for $q\bar{q} \to W^{\pm}\gamma$ and $q\bar{q} \to Z^0\gamma$*, *JHEP* **02** (2012) 004 [arXiv:1112.1531] [INSPIRE].

[123] D. de Florian and J. Mazzitelli, *Two-loop virtual corrections to Higgs pair production*, *Phys. Lett.* **B 724** (2013) 306 [arXiv:1305.5206] [INSPIRE].

[124] T. Gehrmann, A. von Manteuffel and L. Tancredi, *The VVamp project*, http://vvamp.hepforge.org.

[125] J. Alwall et al., *MadGraph/MadEvent v4: the new web generation*, *JHEP* **09** (2007) 028 [arXiv:0706.2334] [INSPIRE].

[126] J.M. Campbell et al., *NLO Higgs boson production plus one and two jets using the POWHEG BOX, MadGraph4 and MCFM*, *JHEP* **07** (2012) 092 [arXiv:1202.5475] [INSPIRE].

[127] G. Cullen et al., *GoSAm-2.0: a tool for automated one-loop calculations within the standard model and beyond*, *Eur. Phys. J.* **C 74** (2014) 3001 [arXiv:1404.7096] [INSPIRE].

[128] W. Astill, W. Bizoń, E. Re and G. Zanderighi, *NNLOPS accurate associated HZ production with NLO decay $H \to b\bar{b}$*, *Submitted to: JHEP* (2018) [arXiv:1804.08141] [INSPIRE].

[129] S. Catani, Y.L. Dokshitzer, M.H. Seymour and B.R. Webber, *Longitudinally invariant K_t clustering algorithms for hadron hadron collisions*, *Nucl. Phys.* **B 406** (1993) 187 [INSPIRE].

[130] S.D. Ellis and D.E. Soper, *Successive combination jet algorithm for hadron collisions*, *Phys. Rev.* **D 48** (1993) 3160 [hep-ph/9305266] [INSPIRE].

[131] M. Cacciari, G.P. Salam and G. Soyez, *FastJet user manual*, *Eur. Phys. J.* **C 72** (2012) 1896 [arXiv:1111.6097] [INSPIRE].

JHEP12(2018)121

[132] A. Denner, S. Dittmaier, M. Roth and L.H. Wieders, *Electroweak corrections to charged-current $e^+e^- \to 4$ fermion processes: Technical details and further results*, *Nucl. Phys.* **B 724** (2005) 247 [*Erratum ibid.* **B 854** (2012) 504] [hep-ph/0505042] [INSPIRE].

[133] PARTICLE DATA GROUP collaboration, C. Patrignani et al., *Review of particle physics*, *Chin. Phys.* **C 40** (2016) 100001 [INSPIRE].

[134] NNPDF collaboration, R.D. Ball et al., *Parton distributions for the LHC Run II*, *JHEP* **04** (2015) 040 [arXiv:1410.8849] [INSPIRE].

[135] T. Sjöstrand et al., *An introduction to PYTHIA 8.2*, *Comput. Phys. Commun.* **191** (2015) 159 [arXiv:1410.3012] [INSPIRE].

[136] LHC HIGGS CROSS SECTION WORKING GROUP collaboration, D. de Florian et al., *Handbook of LHC Higgs Cross Sections: 4. Deciphering the nature of the Higgs sector*, arXiv:1610.07922 [INSPIRE].

[137] E. Bagnaschi, G. Degrassi, P. Slavich and A. Vicini, *Higgs production via gluon fusion in the POWHEG approach in the SM and in the MSSM*, *JHEP* **02** (2012) 088 [arXiv:1111.2854] [INSPIRE].

[138] B. Mistlberger, *Higgs boson production at hadron colliders at N^3LO in QCD*, *JHEP* **05** (2018) 028 [arXiv:1802.00833] [INSPIRE].

[139] C. Anastasiou et al., *High precision determination of the gluon fusion Higgs boson cross-section at the LHC*, *JHEP* **05** (2016) 058 [arXiv:1602.00695] [INSPIRE].

[140] C. Anastasiou et al., *Higgs boson gluon-fusion production in QCD at three loops*, *Phys. Rev. Lett.* **114** (2015) 212001 [arXiv:1503.06056] [INSPIRE].

[141] A. Djouadi, M. Spira and P.M. Zerwas, *Production of Higgs bosons in proton colliders: QCD corrections*, *Phys. Lett.* **B 264** (1991) 440.

[142] S. Marzani et al., *Higgs production via gluon-gluon fusion with finite top mass beyond next-to-leading order*, *Nucl. Phys.* **B 800** (2008) 127 [arXiv:0801.2544] [INSPIRE].

[143] R.V. Harlander, H. Mantler, S. Marzani and K.J. Ozeren, *Higgs production in gluon fusion at next-to-next-to-leading order QCD for finite top mass*, *Eur. Phys. J.* **C 66** (2010) 359 [arXiv:0912.2104] [INSPIRE].

[144] A. Pak, M. Rogal and M. Steinhauser, *Finite top quark mass effects in NNLO Higgs boson production at LHC*, *JHEP* **02** (2010) 025 [arXiv:0911.4662] [INSPIRE].

[145] H. Mantler and M. Wiesemann, *Top- and bottom-mass effects in hadronic Higgs production at small transverse momenta through LO+NLL*, *Eur. Phys. J.* **C 73** (2013) 2467 [arXiv:1210.8263] [INSPIRE].

[146] R.V. Harlander, T. Neumann, K.J. Ozeren and M. Wiesemann, *Top-mass effects in differential Higgs production through gluon fusion at order α_s^4*, *JHEP* **08** (2012) 139 [arXiv:1206.0157] [INSPIRE].

[147] T. Neumann and M. Wiesemann, *Finite top-mass effects in gluon-induced Higgs production with a jet-veto at NNLO*, *JHEP* **11** (2014) 150 [arXiv:1408.6836] [INSPIRE].

[148] E. Bagnaschi et al., *Resummation ambiguities in the Higgs transverse-momentum spectrum in the standard model and beyond*, *JHEP* **01** (2016) 090 [arXiv:1510.08850] [INSPIRE].

[149] H. Mantler and M. Wiesemann, *Hadronic Higgs production through NLO + PS in the SM, the 2HDMand the MSSM*, *Eur. Phys. J.* **C 75** (2015) 257 [arXiv:1504.06625] [INSPIRE].

[150] M. Buschmann et al., *Mass effects in the Higgs-gluon coupling: boosted vs. off-shell production*, *JHEP* **02** (2015) 038 [arXiv:1410.5806] [INSPIRE].

JHEP12(2018)121

[151] R. Frederix, S. Frixione, E. Vryonidou and M. Wiesemann, *Heavy-quark mass effects in Higgs plus jets production*, *JHEP* **08** (2016) 006 [arXiv:1604.03017] [INSPIRE].

[152] S. Höche, Y. Li and S. Prestel, *Higgs-boson production through gluon fusion at NNLO QCD with parton showers*, *Phys. Rev.* **D 90** (2014) 054011 [arXiv:1407.3773] [INSPIRE].

[153] S. Catani and B.R. Webber, *Infrared safe but infinite: soft gluon divergences inside the physical region*, *JHEP* **10** (1997) 005 [hep-ph/9710333] [INSPIRE].

[154] LHCb collaboration, *Measurement of forward $W \to e\nu$ production in pp collisions at $\sqrt{s} = 8$ TeV*, *JHEP* **10** (2016) 030 [arXiv:1608.01484] [INSPIRE].

JHEP12(2018)121